Hydrogen Bonding—New Insights

Edited by

SŁAWOMIR J. GRABOWSKI

Department of Physics and Chemistry
University of Łódź
Poland

Springer

A C.I.P. Catalogue record for this book is available from the Library of Congress.

ISBN-10 1-4020-4852-1 (HB)
ISBN-13 978-1-4020-4852-4 (HB)
ISBN-10 1-4020-4853-X (e-book)
ISBN-13 978-1-4020-4853-1 (e-book)

Published by Springer,
P.O. Box 17, 3300 AA Dordrecht, The Netherlands.

www.springer.com

Printed on acid-free paper

CONTENTS

CHAPTER 10

POTENTIAL ENERGY SHAPE FOR THE PROTON MOTION IN HYDROGEN BONDS REFLECTED IN INFRARED AND NMR SPECTRA

GLEB S. DENISOV[1], JANEZ MAVRI[2] and LUCJAN SOBCZYK[3,*]

[1] *Institute of Physics, St. Petersburg State University, Petrodvorets, Ulyanowskaya 1, 198504 Sankt Petersburg, Russia;* [2]*National Institute of Chemistry, Hajdrihova 19, SL-1000 Ljubljana, Slovenia;* [3]*Faculty of Chemistry, University of Wroclaw, Joliot-Curie 14, 50–383 Wroclaw, Poland*

Abstract The importance of the shape of the potential for the proton motion in hydrogen bonds is emphasized in various molecular phenomena. There are discussed such problems as anharmonicity, empirical equations describing potentials, variational solutions of the Schrödinger equation, Car–Parrinello simulation and quantum-dynamical simulation of the proton motion. Critical review is presented with respect to the relationship between the anharmonic potential energy shape and infrared spectra. Possibilities of application of NMR spectra with various nuclei are presented as applied to complexes of neutral molecules and with participation of ions. An attention is also paid to intramolecular hydrogen bonds in such systems like enols of β-diketones.

Keywords: Potential for the proton motion; theoretical treatment; anharmonicity and IR spectra; NMR spectra.

1 INTRODUCTION

The shape of the potential for the proton motion, particularly when the proton is engaged in hydrogen bond formation, is one of the most fascinating problems of molecular physics and chemistry. Because of very low mass the stretching protonic vibrations are characterized by high frequencies and, if independent of additional interactions, they are anharmonic. It is commonly known that expression of quantum-chemical calculations in the harmonic approximation, on various levels of the quantum-mechanical approach, needs the application of some scaling factors [1, 2]. For stretching protonic vibrations this factor is

* L. Sobczyk is the corresponding author.

S. Grabowski (ed.), Hydrogen Bonding—New Insights, 377–416.

less than unity: where the calculated frequencies are markedly higher than the experimental ones. The hydrogen bond interaction increases these effects.

The anharmonicity of the stretching protonic vibrations has several effects specific in character for hydrogen bonds. In particular, it leads to coupling with low frequency modes, arising from the bridge stretching vibrations. This phenomenon is of great importance in the relaxation of excited vibrational levels, and thus in broadening of IR bands and in the formation of the substructure of these bands [3]. It also results in the coupling of protonic stretching vibrations with overtones and summation frequencies of modes in the medium frequency range below $1800\,cm^{-1}$, particularly those which the δ(AH) and γ(AH) protonic deformation vibrations contribute.

In the case of a very strong hydrogen bond the situation becomes much more complicated, in particular when we approach the so-called critical region where a double minimum potential appears. A variety of situations are illustrated in Fig. 1 for the simplified one-dimensional model.

One can expect that particular situation should appear for the double minimum potential with very low barrier. The anharmonicity of the potential in such a critical region is unusual; it can be opposite to that observed in usual hydrogen bonded systems. On the other hand, it is commonly accepted

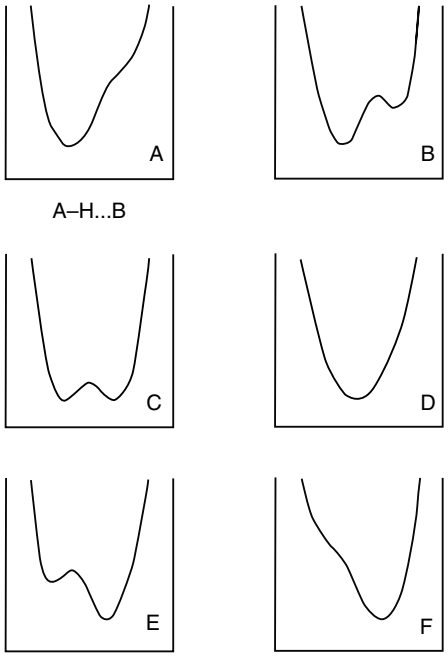

Figure 1. Various one-dimensional potential energy curves for the proton motion in AH···B hydrogen bonds.

that low-barrier hydrogen bonds are of great importance in chemistry and enzymology [4]. They will be one of the main topics to be discussed in this chapter.

There are a plethora of isotope effects accompanying hydrogen bond formation [5]. Isotopic substitution leads to a substantial decrease of anharmonicity of stretching vibrations, while also producing major effects when the barrier height is lowered. In this case the fundamental vibrational level is lowered with respect to the barrier top and a marked reduction of the tunnelling effect takes place.

In this review we would like to focus on three main topics:

- Theoretical aspects of the potential energy surface (Sects. 4–7).
- Correlation of infrared spectra with the shape of the potential (Sects. 8–10).
- NMR spectra of hydrogen bonded systems (Sects. 11–14).

The approaches described in Sects. 4–7 and the analytical approaches in the subsequent sections are complementary. Construction of the multidimensional hypersurface on medium high ab initio or DFT level and solving the vibrational Schrödinger equation require several thousand hours of CPU time. The obtained expectation values are reliable and usually compare well with the experiment. The approach may, however, be classified as a numerical experiment since there are no analytical solutions.

The application of one-dimensional model potentials provides many insights and helps predict trends, which can be of significant benefit to experimentalists rationalizing their measurements and in designing new experiments.

2 EMPIRICAL EQUATIONS DESCRIBING ONE–AND TWO–DIMENSIONAL POTENTIALS

The one-dimensional potential energy curve describes precisely the electronic term of a system only in the simple case of diatomic molecules. With A–H bonds, where A is part of a multiatom molecule, the diatomic approximation is valid. But in the general case the potential energy as a function of the A–H bond length, $V(r)$, should be expressed using a polynomial expansion

$$V(r) = V(r_e) + \left(\frac{\partial V}{\partial r}\right)_{r=r_e}(r - r_e) + \frac{1}{2!}\left(\frac{\partial^2 V}{\partial r^2}\right)_{r=r_e}(r - r_e)^2 + \frac{1}{3!}\left(\frac{\partial^3 V}{\partial r^3}\right)_{r=r_e}(r - r_e)^3 + \cdots \quad (1)$$

where r_e is the equilibrium bond length. The first non-zero square component of the polynomial has the parabolic shape that corresponds to the harmonic potential. However, the A–H bond, especially when forming the hydrogen bond, can never be approximated by a harmonic potential; and higher terms of the polynomial (i.e. cubic, etc.) corresponding to anharmonic potentials should be taken into account. The real potential may also be approximated

by simple functions based on experimental data or on quantum-chemical calculations of the energy for varying r.

The Morse potential, the oldest, and to date the most widely applicable expression, is presented for the diatomic molecule in the form

$$V(r) = D_e[1 - \exp(-a(r - r_e))]^2 \quad (2)$$

where constants D_e and a express the depth and width of the potential well, and r_e is the equilibrium distance. The comparison of the harmonic potential with the real anharmonic potential is shown in Fig. 2, where D_o is the dissociation energy and D_e is the bond energy. The Morse potential is much more realistic than the potential function described in the harmonic approximation. The chemical bond described by the Morse function can dissociate. A combination of Morse functions is the basis for the empirical valence bond (EVB) method, which can realistically describe parts of the Born–Oppenheimer (BO) surface responsible for chemical reactivity [6].

The Morse function describes quite satisfactorily the potential where $r > r_e$, but it is less reliable where $r < r_e$ because there is a strong repulsion at small interatomic distances.

A somewhat modified version of the Morse potential was proposed [7] in the form

$$V(r) = D_e[1 - \exp(-n(r - r_e)^2/2r)] \quad (3)$$

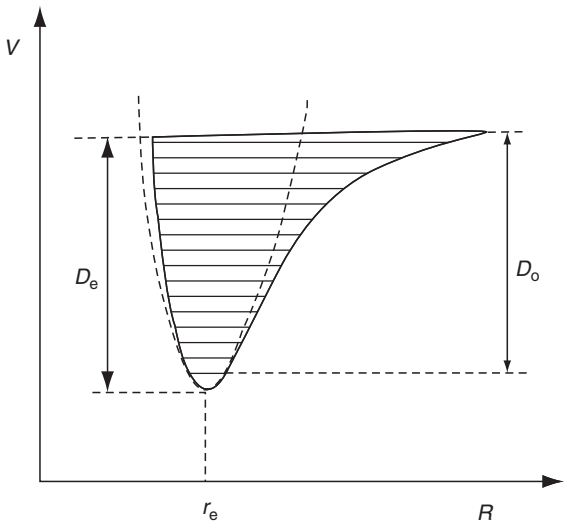

Figure 2. Harmonic (dashed curve) vs. real anharmonic potential $V(r)$ with vibrational levels; r_e is equal to the equilibrium distance.

where the coefficient $n = k_e r_e / D_e$ replaces the parameter a (k_e is the force constant of the stretching vibrations). The diatomic approximation is applicable to AH stretching vibrations, since they can be described as a separate mode due to small mass of a proton and high frequency.

For strong hydrogen bonds a second potential minimum appears, and that leads to a substantial modification of the potential energy curve. The simplest solution of the problem was the application of the double Morse function [8], shown in the form

$$V(r) = D_e\{\exp[-2a(r - r_e)] - 2\exp[-a(r - r_e)]\} \tag{4}$$

This has been applied successfully to the analysis of tunnelling phenomena and isotope effects in strongly hydrogen-bonded crystals.

The best description of the one- and the two-dimensional potential is the Lippincott–Schröder equation [7]. The Lippincott–Schröder function consists of three parts assigned to three interaction components V_1, V_2, V_3, respectively, A–H, B^+–H (proton transfer state) and A···B:

$$\begin{array}{c} V(r',\, R) = V(r') + V_2(r',\, R) + V_3(r',\, R) \\ \qquad\qquad\quad \downarrow \qquad \downarrow \qquad\quad \downarrow \\ \qquad\quad \text{A–H} \quad \text{B}^+\text{–H} \qquad \text{A}\cdots\text{B} \end{array} \tag{5}$$

The geometrical parameters used in the description of the above components are presented in Fig. 3.

The values of particular components are expressed in the following equations:

$$V_1(r') = D\left[1 - \exp\left(\frac{-n(r - r_\circ \cos\alpha^2)}{2r' \cos\alpha}\right)\right] \tag{6}$$

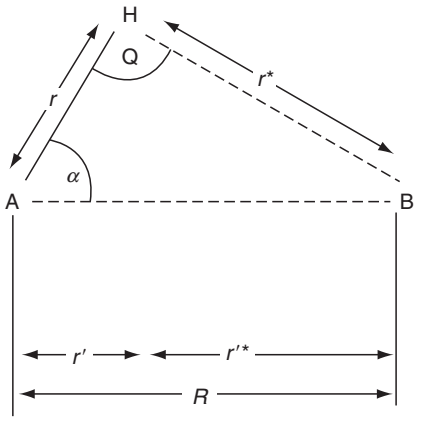

Figure 3. Geometrical parameters used in the Lippincott–Schröder equation.

$$V_2(r',\ R) = -D\left[\frac{n^*[R - r - r_\circ^* \cos(\alpha + \Theta)]^2}{2(R - r')\cos(\alpha + \Theta)}\right] \tag{7}$$

$$V_3(r',\ R) = A(r')\exp(-bR_\circ)\left\{\exp\left[-\mathrm{b}(R - R_\circ) - \frac{1}{2}(R_\circ/R)^m\right]\right\} \tag{8}$$

while

$$A(r') = -n^* D^*\left\{1 - [r_\circ^*/(R_\circ - r')]^2\right\}\exp\left[\frac{n^*[R_\circ - r' - r_\circ^* \cos(\alpha + \Theta)]^2}{2(R_\circ - r')\cos(\alpha + \Theta)}\right] \times [2\cos(\alpha + \Theta)\exp(-bR_\circ)(b - m/2R_\circ)]^{-1}$$

where, $n = k_\mathrm{o} r_\mathrm{o}/D$($k_\mathrm{o}$ is the force constant of vibration of the free A–H group); $n^* = k^* r^* D^*$, and is related to the B^+–H group; D and D^* are the A–H and B^+–H bond energies; b represents the repulsion between A and B while the exponent m is close to unity.

The parameter values of the Lippincott–Schröder equation for the three most common types of hydrogen bonds are summarized in Table 1 [9].

The usefulness of Lippincott–Schröder potential was shown, e.g., in studies of isotope effects and vibrational levels [10].

The fourth-order polynomial proposed for the first time by Somorjai and Hornig [11] appeared to be useful in semiquantitatvie analysis, and can be expressed in the general form

$$V(r,\ R) = a_2(R)r^2 + a_3(R)r^3 + a_4(R)r^4 \tag{9}$$

where R is the bridge coordinate (the A···B distance) and r is the A–H distance. The coefficients a_2, a_3, a_4 are normally a function of R. The first component of the equation expresses the harmonic potential with a single minimum, while the third component presents a symmetrical double minimum potential. The second component describes the asymmetry of the potential. The coefficients a_2 and a_4 can be fitted to experimental spectroscopic correlations for particular types of hydrogen bonds [12]. The equation was successfully applied in a semiquantitative analysis of IR spectra of hydrogen bonded systems [13, 14]. A simple double minimum potential was proposed by Laane [15] in studies on the influence of the

Table 1. Values of the Lippincott–Schröder potential parameters for OH···O, NH···O and N-H···N hydrogen bonds

	OH···O	NH···O	NH···N
D (kcal · mol^{-1})	118.6	112.4	112.5
n (10^8 cm^{-1})	9.18	8.60	9.01
n^* (10^8 cm^{-1})	13.32	13.15	13.49
r_o (A)	0.97	0.99	1.033
r_o^* (A)	0.97	0.97	1.038
b (10^8 cm^{-1})	4.8	4.8	4.8

barrier height on the IR spectroscopic behaviour of hydrogen bonds. A detailed analysis of the hydrogen and proton transfer processes in hydrogen bonded systems was recently performed based on the modified Lippincott–Schröder potential [16]. This showed good agreement of calculated barrier heights with experimental data and with advanced ab initio calculations.

3 EMPIRICAL VALENCE BOND APPROACH

Ab initio and DFT calculations of the BO surfaces, which are used to describe hydrogen-bonded systems, are computationally demanding. Computational practice has shown that a flexible basis set is required. The Hartree–Fock (HF) level is typically insufficient, and electron correlation must be included. DFT is an attractive alternative to the post HF calculations. The hypersurface is obtained in such a way pointwise. One can fit it to a computationally efficient form that allows for an inexpensive evaluation needed in thermal averaging or calculation of matrix elements when performing vibrational analysis.

The EVB method proposed by Warshel [6] is an elegant and computationally very efficient method of describing the entire BO surface, thus allowing treatment of chemical reactions such as proton transfer in hydrogen bonds. It can also be used in vibrational analysis. In conjunction with the environment described at the molecular mechanics level it was the first QM/MM method. Vibrational analyses of hydrogen bonded systems and of enzymatic catalysis have a lot in common.

In both cases it is necessary to describe parts of the hypersurface relatively high above the minimum. In a typical enzymatic reaction proton transfer is associated with the rearrangement of covalent bonds, where the free energy of activation is about $20\,\mathrm{kcal}\cdot\mathrm{mol}^{-1}$. The vibrational transition $0\rightarrow1$ in a hydrogen bond has an OH stretching frequency of $3000\,\mathrm{cm}^{-1}$ with a ground vibrational state at $4.3\,\mathrm{kcal}\cdot\mathrm{mol}^{-1}$ and the first excited state at around $12.9\,\mathrm{kcal}\cdot\mathrm{mol}^{-1}$. In EVB the system wave function is represented by two or more resonant forms.

A proton transfer across a heteronuclear hydrogen bond can typically be represented with two resonant forms; one corresponding to the neutral state and the second one corresponding to the ionic state. In the EVB approach a Hamiltonian matrix is constructed. Diagonal matrix elements are usually described by Morse functions, while the off-diagonal elements are either constants or distance dependent functions. Hamiltonian diagonalization gives rise to eigenstates and eigenfunctions. EVB has strong transferability, which is essential for computational support of biocatalysis. Nuclear quantum effects can be easily studied by EVB, since matrix elements necessary for quantum treatment of nuclei can be calculated with minimal CPU time. EVB has been used frequently in studies of hydrogen-bonded systems, including proton transfer reactions in enzymes. For a recent discussion concerning EVB and closely related methods see Ref. [17].

4 VARIATIONAL SOLUTIONS OF THE SCHRÖDINGER EQUATION

Hydrogen bonded systems are highly anharmonic and therefore their computational treatment in a harmonic approximation is of very limited value. On the other hand, rapid progress in advanced experimental techniques, such as the pulse-echo treatment of hydrogen bonding dynamics, requires computational support that should, ideally, be state-resolved. The ideal solution would consist of a numerical solution of the time-dependent Schrödinger equation (SE) for the nuclei. The time-independent SE still provides solutions that are of high value for the interpretation of experimental data. Thus, they are useful for the interpretation of vibrational spectra, or for H/D isotope effects on the chemical shift of hydrogen bonded systems.

A software program was developed for variational solutions of the time-independent SE in one and two dimensions [18]. Extension to more dimensions is straightforward. The first part of the program includes the fitting program (FIT), which allows points calculated by ab initio or DFT to be fitted to a computationally efficient and functional form. Proper fitting of the potential energy surface is crucial for the quality of the results. The second part of the program provides for the variational solution of the 2D Schrödinger, using either a shifted Gaussian basis set or a rectangular basis set [19]. The third part of the program calculates the expectation values, includes IR and Raman spectra (XPECT) and plots the results (PLOT). This program was applied to study the nature of the strong hydrogen bond in picolinic acid N-oxide (Fig. 4).

Potential energy surfaces calculated by ab initio or DFT are fitted to various functional forms that include: polynomial expansion, linear combination of Gaussians, splines and an EVB form. Proper fitting of the potential energy surface is essential for the calculated eigenvalues and eigenfunctions. In the case of picolinic acid N-oxide we have found satisfactory representation of the two-dimensional potential energy surface (2D PES) by a superposition of about ten shifted Gaussians. Shifted Gaussians or local constants on a rectangular grid were used as basis functions for the variational solution. As a criterion of reliability a given number of eigenvalues below the energy threshold were applied. Several test runs were performed on harmonic oscillators and on the intramolecular strong hydrogen bond in PANO. Only in nearly harmonic systems is the Gaussian basis set more favourable than the grid basis set in terms of CPU time and memory usage. For realistic, anharmonic systems it has been demonstrated that the grid basis set has several advantages over the Gaussian basis set:

- The potential part of the Hamiltonian matrix is diagonal. This becomes important if the potential energy matrix elements are not analytical.
- For sufficiently fine grids, the integration of the potential energy matrix elements can be approximated by the potential function above the centre of the basis function.

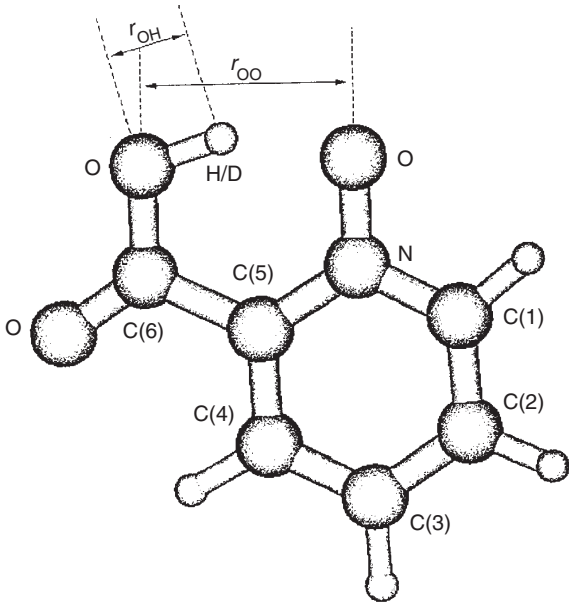

Figure 4. Structure and atom numbering in picolinic acid *N*–oxide.

– The grid basis set requires no orthogonalization. On the other hand, canonical orthogonalization with the Gaussian basis set requires overlap matrix diagonalization and one matrix multiplication.
– The grid basis set procedure is much easier to code.

With multidimensional problems, the grid basis set is more suitable for matrix diagonalization procedures, which yield a desired number of the lowest eigenvalues. Extension of the procedure to three and more dimensions is straightforward.

At this point it is worth emphasizing that the amount of CPU time required to construct the hypersurface depends exponentially on the number of dimensions. If ten points are required for each dimension then for a four-dimensional problem one would need 10,000 points, which is not a computationally trivial problem. Matrix operations involving such large matrices are also not trivial, both in terms of memory and CPU time.

It will be a challenge for the future to solve the Hadžis ABC trio of a strong hydrogen bonded system, representing a four-dimensional problem.

5 CALCULATION OF NMR ISOTOPE EFFECTS

Chemical shifts are the most important molecular responses to external magnetic fields. Chemical shift calculations are extremely sensitive for the applied level of theory. Calculated shift assist the interpretation of the NMR spectra of complex organic compounds [20–25].

In the case of strong hydrogen bonds a quantum nature of the proton motion adds additional complexity to the problem. Obviously, deuteration gives rise to different nuclear wave function for the hydrogen bond motion resulting in changed expected values that include chemical shifts. Traditionally computational studies concerning chemical shift isotope effects were limited only to one dimension: only OH stretching coordinate was concerned. In a recent study the approach to two dimensions was performed [26]. Beside isotopic substitution, the solvent effect was also considered: experiments were performed in chloroform and acetonitrile solution. The effects of solvation were taken into account using the solvent reaction field method of Tomasi and Persico [27]. It is worth emphasizing that the so-obtained hypersurfaces have meaning of free energy hypersurfaces as shown in Fig. 5. To summarize the work, the two-dimensional free energy and chemical shift hypersurfaces were constructed along the OH and OO internal coordinates that are of major importance for the structure and dynamics of hydrogen bonding in PANO. The anharmonic vibrational wave functions and their energies were calculated and used then in the thermal quantum averaging of the chemical shift functions. With minor exceptions, fairly good agreement between the calculated and experimental chemical shifts was found, especially for the relative values, signs and trends of the solvent effect and the isotope effects on chemical shifts. In particular, a good agreement between the experiment and the absolute values for the primary isotope effect was found. Some of the calculated values are in rather poor agreement with the

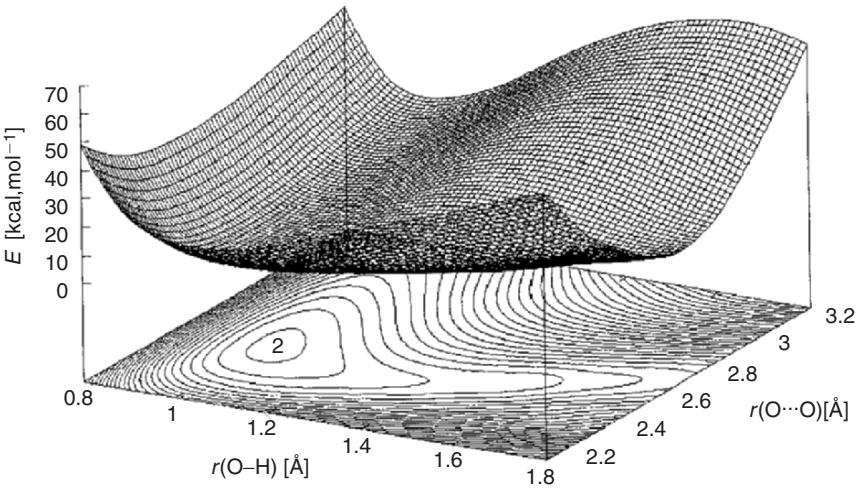

Figure 5. Free energy surface for picolinic acid *N*-oxide in chloroform solution as a function of OH and OO distances calculated on the B3LYP/6–31+G(*d*,*p*) level. Solvent reaction field method of Tomasi and Persico was used to calculate the free energy of solvation. The applied dielectric permitivity was 4.9.

experiment; this can possibly be attributed to limitations of the applied methods, including the B3LYP functional, the reaction field model and the limited number of vibrational degrees of freedom taken into account. In our study the vibrational SE was solved for the free energy hypersurface. In principle such an approach is methodologically questionable, since the quantization of fast vibrational degrees of freedom is performed over averaged solvent orientational polarization that is at least two orders of magnitude slower. This problem is associated not only with the present approach but is inherent to solvent reaction field in general in the context of solute electron motion vs. solvent dynamics. One believes that the explicit solvent treatment using a QM/MM scheme would improve the results, but we are aware that such an approach would be very CPU demanding. It is definitively a method of choice when dealing with isotope effects in hydrogen bonds in complex environments such as enzymes. All in all our experiment and calculations yield evidence that the hydron distribution in the hydrogen bond has a significant influence on the chemical shifts of all the carbon atoms in the investigated compound. It is illustrated for the C3 atom in Fig. 6.

We are sure that measurements of chemical shifts and associated computational support will play a very important role in the studies of enzyme active sites like in Ref. [28].

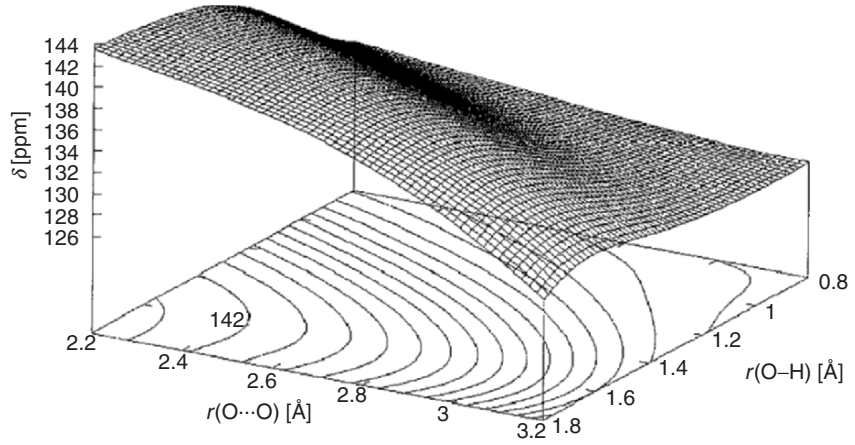

Figure 6. Chemical shift of the C3 atom as a function of OH and OO distance in picolinic acid *N*-oxide, according to Ref. [26]. Reprinted from Ref. [26] by permission granted by the American Chemical Society. For each OH and OO value all other geometry parameters were optimized. The inner contour labelled "2" pertains to the energy value of $2\,\mathrm{kcal}\cdot\mathrm{mol}^{-1}$ above the minimum; successive contours are drawn at $2\,\mathrm{kcal}\cdot\mathrm{mol}^{-1}$ intervals. according to Ref. [26].

6 CAR–PARRINELLO SIMULATION OF THE STRETCHING AH VIBRATIONS

In this section preliminary results of the Car–Parrinello molecular dynamics of PANO in the solid state are reported [29]. In particular, we are interested in simulation of the broad band associated with the OH stretching motion.

The Car–Parrinello method belongs to the class of the methods called ab initio molecular dynamics. These methods solve equations of motion for atomic nuclei, where the forces are calculated quantum-mechanically. The most widely used theory for studying the quantum-mechanical electronic structure problem of solids and larger molecular systems is the density-functional theory of Hohenberg and Kohn in the local-density approximation (LDA). Car and Parrinello's method [30] is based on the LDA, and uses pseudopotentials and plane wave basis sets, but they added the concept of updating iteratively the electronic wave functions simultaneously with the motion of atomic nuclei (electron and nucleus dynamics are coupled). This is implemented in a standard molecular dynamics paradigm, associating dynamical degrees of freedom with each electronic Fourier component with a small mass. The procedure turned out to be very efficient, especially for the large systems.

The application of the plane wave basis set implies that the periodicity is taken into account and the method is therefore well suited for the simulation of the crystal field effects. For a recent review of Car–Parrinello methodology see Ref. [31]. With Car–Parrinello method the proton motion in PANO including the effects of crystal environment was simulated. The molecular dynamics simulation was carried out at a constant volume, i.e. the unit cell parameters were fixed during the simulation. Fictitious orbital mass was set to 150 a.u. (note that 1 a.u. corresponds to the electron mass) and the propagation time step was set to 2 a.u.

The temperature of the system was controlled using the Nose–Hoover thermostat for the nuclear motion. Target temperature was set to 300 K. The structure of PANO was energy minimized prior to the dynamics run. The simulation consisted of about 300,000 steps, the simulated time was approximately 14.5 ps. Nuclear coordinates were saved to the trajectory file every time step of the simulation. Next, snapshots of the dynamics were extracted from the trajectory every 5,000 steps (approx. 242 fs). In such a way, 50 distinct structures, as generated by the dynamics simulation, were obtained. From each of these structures, two proton potential functions (one per PANO molecule in the unit cell) were acquired by stepwise displacing the H-bonded proton along the line that connects the proton donor and the oxygen nucleus while keeping all the other nuclei frozen; a single point calculation was performed for each proton position. A total number of 100 proton potentials were obtained in such a way.

Anharmonic vibrational energies and wave functions were determined for each of these potentials by solving the vibrational SE. The variational Fourier

Grid Hamiltonian method was used for this purpose. The calculated anharmonic OH stretching frequencies are distributed over a wide range between 1,100 and 2,100 cm^{-1}. The frequency of each individual 0 to 1 vibrational transition is represented as a delta function whose height is proportional to the dipole-driven transition intensity in the approximation of electric harmonicity. The distribution of the frequencies outlines the shape of the broad band attributed to the OH stretching mode. The envelope shown in Fig. 7 was obtained by representing each individual transition as a Gaussian function of a half-width of 50 cm^{-1} centred at the pertinent frequency. Each of the Gaussians was scaled in such a way that its integral was equal to the calculated transition intensity. The calculated envelope of the OH stretching band spans over a very wide range and at least qualitatively matches the experimental broad absorption in the experimental infrared spectrum of solid PANO that is attributed to the OH stretching mode. The peak of the band at about 1,400 cm^{-1} is in good agreement with the estimated centre of the experimental broad absorption [32].

At this point it is worth to emphasize that the spectrum calculated from the velocity autocorrelation function is in disagreement with the experiment. The

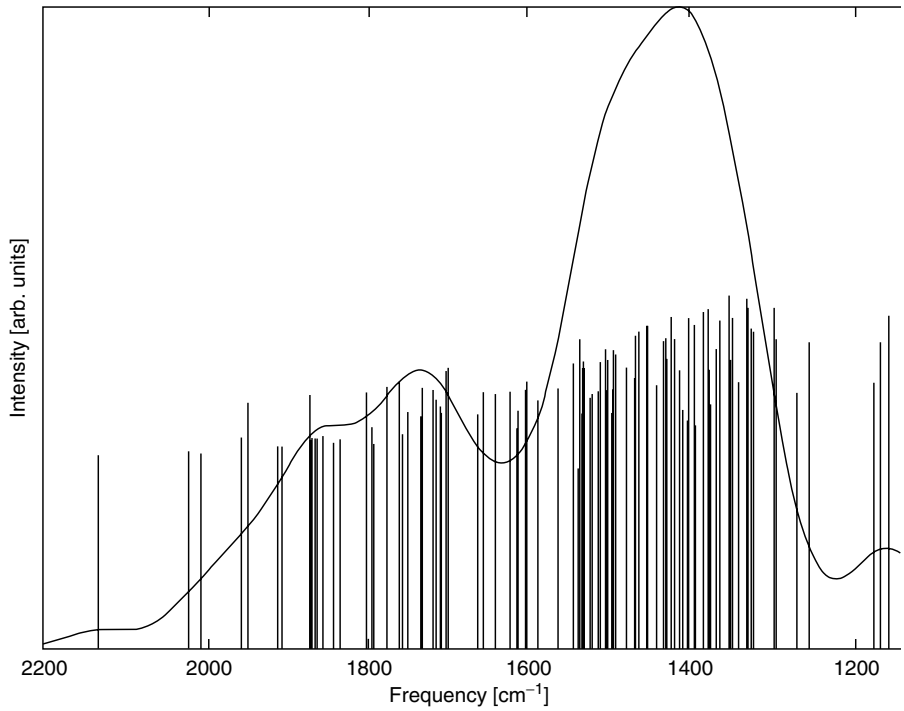

Figure 7. Car–Parrinello calculated envelope for the OH stretching mode in picolinic acid N-oxide in the solid state, according to Ref. [32].

applied methodology can be easily applied to study spectra of hydrogen bonds in solution or in a fluctuating macromolecular environment. Computational costs associated with evaluation of the force and energies, however, still prevent quantum-dynamical simulation of the proton motion using the Car–Parrinello methodology.

7 QUANTUM-DYNAMICAL SIMULATION OF THE PROTON MOTION

In this section we report quantum-dynamical simulation of the proton motion in acetylacetone. Acetylacetone is a medium strong hydrogen bonded system with the OH asymmetric stretching frequency band centred at $2800\,cm^{-1}$. The system is conjugated, giving rise to weak OH stretching frequency band. The band we simulated using the following strategy. First computationally inexpensive functional form of the potential was constructed. The one-dimensional OH motion was treated by time-dependent SE, while, the rest of the system, including solvent, was treated on the level of molecular mechanics. The density matrix evolution (DME) method is coupled with classical systems [33]. The DME method is based on the coupling of the Liouville–von Neumann equation with which the quantum subsystem is described with the classical equations of motion. For the quantum subsystem a few displaced Gaussian functions are used, what formally corresponds to the application of Gauss–Hermite polynomials that are eigenfunctions for harmonic oscillator. The force acting on the classical subsystem is just its expectation value. The DME method can be contrasted with the surface hopping method where the force originates from the pure quantum states, giving rise to the ad hoc scaling of the velocities of the classical particles in order to preserve the total energy.

The spectrum was calculated from the time-dependent wave function of the proton wave function. The proton potential in acetylacetone was first examined by semiempirical MO methods, ab initio methods on the HF and MP2 levels, and by the DFT method using the exchange functional proposed by Becke and the correlation functional of Lee, Yang and Parr. The semiempirical method yields an unreasonably high barrier to the proton transfer. The Hartree–Fock calculations also yield a too high barrier. The MP2 and B3LYP applied with large, flexible basis sets yield a classical barrier of under $3.0\,kcal \cdot mol^{-1}$. The part of the hypersurface relevant for the proton transfer was explored with the B3LYP/6–311+G(2*d*,2*p*) method yielding a classical barrier of $2.12\,kcal \cdot mol^{-1}$. Variations in the proton potential with respect to the OO distance and both CO distances were considered. The former influences the barrier height, while the latter introduces asymmetry. The potential was fitted to the two state empirical valence form suitable for quantum-dynamical molecular simulations.

Mixed quantum–classical simulation using the DME method was performed in the gas phase and in a chloroform solution [34]. The effects of deuteration were also considered. The vibrational spectrum was calculated by Fourier

transform of the time-dependent expectation value for the OH bond length. In the present case, we demonstrate by calculations and experimentally that coupling of the proton to the OO and both CO bonds, which are attached to the hydrogen bond (indirect relaxation mechanism), is more important than coupling to the solvent degrees of freedom in determining spectral shape.

The DME method has many possible applications. Inclusion of the external electromagnetic field into the mixed quantum–classical simulation is possible and offers a possibility for computational support of the pulse-echo experiments in the infrared region. See for example Ref. [35].

We hope to apply this method in the near future for enzymatic active centres. Replacement of the polar solvent with a fluctuating macromolecular environment, such as an enzyme, is methodologically a straightforward step but requires a lot of coding efforts. Quantum treatment of the nuclear motion is essential for calculation of the kinetic isotope effects that are of vital importance for enzymology. Very recently the H/D kinetic isotope effect $k_H/k_D = 80$ was simulated with what is in excellent agreement with the experiment [36].

8 MAIN FEATURES OF IR SPECTRA RELATED TO THE ANHARMONIC POTENTIAL ENERGY SHAPE

One of the most important parameters characterizing the specificity of hydrogen bondings and affecting the spectroscopic behaviour of hydrogen-bonded systems is the anharmonicity of ν(A–H) vibrations. According to Sándorfy [37, 38] the anharmonicity of ν(A–H) stretching vibrations is defined as being limited to the first overtone. The sign of the X_{12} value is assumed sometimes to be reversed. The data related to the higher order excitations are limited and very rarely discussed:

$$X_{12} = \nu_{01}(\mathrm{AH}) - \frac{1}{2}\nu_{02}(\mathrm{AH}) \tag{10}$$

The importance of anharmonicity of ν(AH) vibrations results first of all from the interpretation of the width and shape of the IR absorption bands. It is almost commonly accepted that the anharmonicity is a source of the coupling phenomena of ν(AH) vibrations with the low frequency vibrations, mainly of the bridge stretching mode and modes into which the bridge atoms contribute. The theoretical basis for the coupling phenomena was formulated by Marechal and Witkowski [39, 40] and developed taking into account the Fermi resonances by Wójcik [41]. The Fermi resonance is of great importance in analysis of the substructure of the broad absorption which is ascribed to the coupling with overtones and combination modes into which the δ(AH) and γ(AH) vibrations contribute.

Wójcik and coworkers [42] studied in particular the band shape for asymmetric OH stretching vibrations in benzoic acid dimer. The experimental spectra were compared with calculated ones. The calculations were based on

the adiabatic coupling between the high frequency mode (OH), the low frequency mode (OO), resonance between the two hydrogen bonds in the dimer and Fermi resonance between the fundamental asymmetric OH stretching and the overtone of the δ(OH) bending vibration. Good agreement between the calculated and experimental results for both OH and OD spectra was found.

As follows from the recently performed analyses [3] the shape of the ν(AH) IR absorption bands results usually from the indirect relaxation of the excited vibrational levels, i.e. through the coupling with the low frequency internal modes which next interact with phonons of the condensed phase. The broad bands are characteristic not only for condensed phases. They are also observed in the gas phase in the case of bulky expanded molecules, which can be treated as a bath. In this case a crucial is the coupling of ν(A–H) vibrations with low frequency bridge vibrations.

As an example of hydrogen-bonded molecules which play the role of a bath in relaxation of the excited ν(A–H) vibrational level can be the dimers of phosphinic acids studied in the gas phase at high temperatures [43]. In Fig. 8 the results of investigations of profiles of broad IR bands ascribed to ν(OH) vibrations with characteristic Hadži's ABC trio are shown. These spectra are very similar to those recorded for strong hydrogen bonds in condensed phases [44].

The example of phosphinic acids illustrates very well the appearance of three submaxima on the envelope of broad bands (continua). Let us note that till now

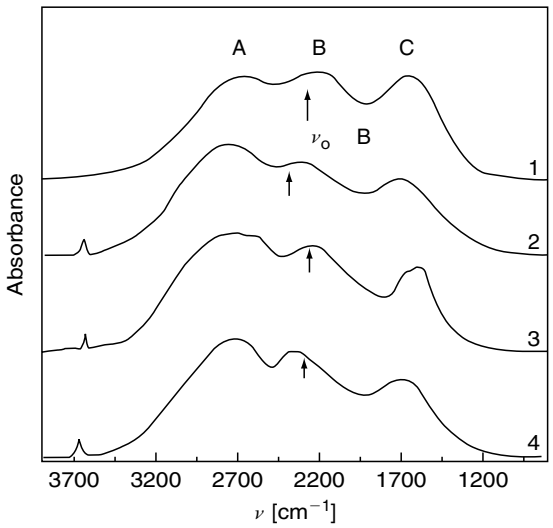

Figure 8. The ν(OH) bands of R_2POOH dimers in the gas phase: 1—H_2POOH (T = 345 K); 2—$(CH_3)_2POOH$ (530 K); 3—$(CH_2Cl)_2POOH$ (450 K); 4—$(C_4H_9O)_2POOH$ (425 K). The arrows denote the centre of gravity ν_o of the dimer band, A, B, C denote the components of ABC structure, reprinted from Ref. [43] by permission granted by the Polish Chemical Society.

there is no commonly accepted view with respect to the origin of submaxima or, as many authors believe, two subminima. The latters could correspond to the Fermi resonance with overtones of δ(OH) and γ(OH) vibrations. One should mention here that Zundel [45] has shown that the broad continuum with submaxima can be due to the overlapping of a few transitions resulted from the tunnel splitting for an asymmetric potential energy curve. A confirmation of the rightness of such a point of view could be considerations of Sokolov [46] on the isotope effect which will be discussed later.

In line of the Zundel approach results of calculations for OHO hydrogen bonds based on Eq. 9 could be considered [12, 13]. In calculation it has been assumed, in agreement with commonly accepted theory of the coupling between anharmonic protonic vibrations with the bridge vibrations, that the relaxation of the excited vibrational states undergoes through such low frequency vibrations. However, it has been assumed simultaneously that the bridge vibrations are strongly damped, particularly in condensed phases due to the interaction with phonons. This assumption is consisted with the stochastic model [47] which implies that the hydrogen bond length is modulated over the amplitude of vibrations. However, the shape of the potential is modulated too. In consequence we have to take into account modulation of the barrier height and splitting of the vibrational levels.

The coefficients a_2 and a_4 of Eq. 9 were fitted to experimental correlations between the ν(AH) frequency and r(AH) bond length and the bridge length. The coefficient a_3 was defined by using the positions of minima and its value was arbitrarily assumed. The calculations were performed for OHO hydrogen bonds for which there are enough data related to the correlation between ν(OH) and r(OH) and the bridge length.

The evolution of the absorption bands starting from long asymmetric hydrogen bonds to symmetric short ones is shown in Fig. 9. It is seen that separated bands corresponding to various transitions cover the whole infrared region. For short symmetric bridges the probability of the high frequency transitions to higher vibrational level drops almost to zero.

The confrontation of experimental spectra with those predicted in such a way does not provide sufficient agreement. There are several reasons for that. First of all the band widths should be larger when we assume that, in addition to the distribution of the bridge length, additional coupling with other low frequency vibrations takes place, especially with vibrational and translational modes. One should also take into account the direct mechanism of relaxation according to the Zundel polarizability of low-barrier hydrogen bonds [45].

Let us come back to the problem of anharmonicity and its relationship with the hydrogen bond strength and hence the potential energy shape for the proton motion.

There is little known about the correlation between the anharmonicity expressed in Eq. 10 and the interaction strength expressed by concrete parameters, e.g. ΔpK_a. On the other hand, there are in our disposal numerous

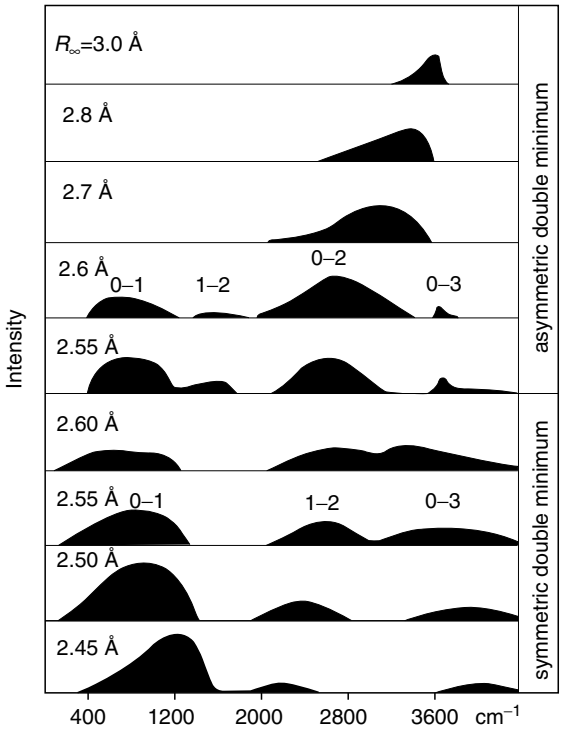

Figure 9. Simulated band profiles for various transitions in OHO hydrogen bonds of varying length, according to Ref. [13].

data related to the $^{1}H/^{2}H$ isotope effects, which can be correlated with the anharmonicity that will be discussed later.

From the data reported by Rospenk and Zeegers-Huyskens [10] related to complexes formed by phenol derivatives and pyridine it follows that for not very high ΔpK_a values X_{12} increases, reaches a maximum and, approaching to the critical region, starts to decrease. The detailed studies performed recently [48] for Mannich bases over broad ΔpK_a region are illustrated in Fig. 10. The results unequivocally show that in the critical point a deep minimum appears and the X_{12} value changes the sign. This clearly reflects a substantial change of the shape of the potential energy curve. It becomes steeper than that of the harmonic one. This behaviour seems to be characteristic for very strong hydrogen bonds. In the case of weak hydrogen bonds, as has been shown in Ref. [49], unexpected minimum of X_{12} value is visible. This phenomenon is illustrated in Fig. 11 for a large number of hydrogen-bonded alcohols. The minimum corresponds to $\Delta\nu$ values of the order of 100 cm^{-1}. Such a behaviour should be considered as due to the coupling of ν(AH) vibrations with δ(AH) and γ(AH) modes which cause the weakening of hydrogen bonds. This result seems to be

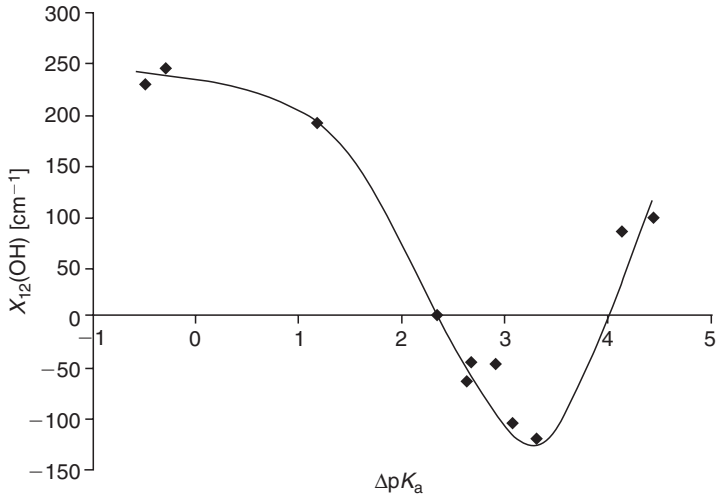

Figure 10. X_{12} values for Mannich bases plotted vs. ΔpK_a, according to Ref. [48].

important in understanding two-dimensional potential energy surfaces. Simultaneously it shows the necessity of taking into account bending vibrations in theoretical analysis.

9 FREQUENCY ISOTOPE EFFECTS

The isotope effects in hydrogen bonded systems reflected in IR spectra were recently reviewed [5]. Here we would like to concentrate our attention on some selected main points.

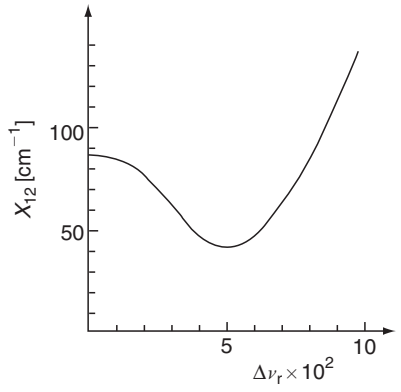

Figure 11. Correlation between the X_{12} value and relative frequency shift $\Delta\nu_r = \Delta\nu(\text{OH})/\nu_o(\text{OH})$ for hydrogen-bonded alcohols, according to Ref. [49].

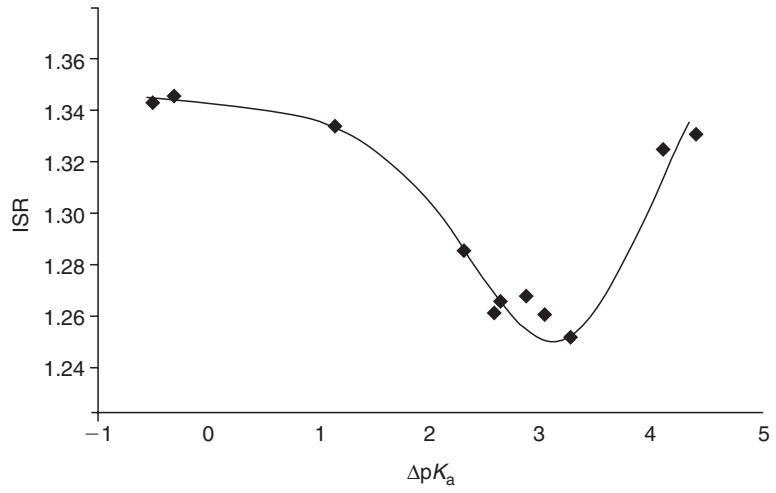

Figure 12. ISR plotted vs. ΔpKa for Mannich bases, according to Ref. [48].

For all systems containing OH···O, OH···N and NH···N hydrogen bonds there are observed deep minima on the plots of isotopic ratio (ISR) = ν(AH)/ν(AD) vs. relative shift of the ν(AH) frequency. This minimum (close to unity) is observed for gravity centre located at 1000–1500 cm^{-1} that is characteristic of strong hydrogen bonds in condensed media. For strongest hydrogen bonds the ISR value starts to increase reaching $\sqrt{2}$ and even more. However, in the case of intramolecular OH···N hydrogen bonds when no continuous broad absorption is observed, the minimum on the plot ISR = $f(\Delta pK_a)$ is not so deep as can be seen in Fig. 12.

This result can speak in favour of the concept that broad continuous absorption extended to very low frequencies is due to overlapping of a few transitions characterized by different isotopic ratio, as argued by Sokolov [46].

In the critical point characterized by a double minimum potential with a low barrier we have to expect high values of ISR markedly exceeding $\sqrt{2}$ that is connected with unusual anharmonicity. An evidence of that are results of studies on the isotope effect in AH complexes with nitrogen bases in low temperature matrices that have been reviewed in Ref. [50]. In the critical point the ISR value markedly exceeds $\sqrt{2}$ while not far from this point the ISR value is evidently lower than $\sqrt{2}$.

10 LOW-BARRIER HYDROGEN BONDS

Some importance in understanding of unusual behaviour of systems with a symmetrical double minimum potential and low barrier possess the results collected recently for charge assisted $[NHN]^+$ bridges, particularly in proto-

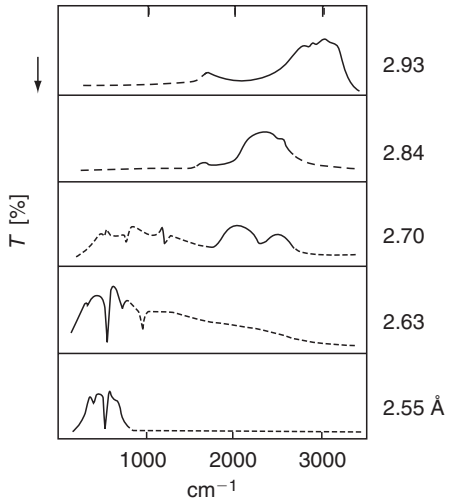

Figure 13. Examples of infrared ν[NHN] bands in NHN hydrogen-bonded systems with different N···N bridge length. The dashed parts of curves were obtained after separation of bands ascribed to other internal modes, based on data cited in Ref. [53].

nated proton sponges [51, 52]. The $\nu[NHN]^+$ absorption bands in protonated naphthalene proton sponges (1,8-*bis*(dimethylamino)-naphthalene (DMAN)), when the symmetric NHN bridges are present, possess unique properties as shown in Fig. 13 comparing with bands corresponding to longer bridges.

For the hydrogen bonds of ca. 2.55 Å length this band is located at extremely low frequencies with an Evans hole assigned to the coupling with NC_3 bending vibrations. For somewhat longer bridges (2.63 or 2.70 Å) a continuous absorption is manifested extending from 100 to 3000 cm^{-1} similarly to those observed for strong OHO or OHN hydrogen bonds. One should mention here that very short charge assisted $[NHN]^+$ hydrogen bonds are constrained by steric effects.

The ab initio and DFT calculations yield the results consistent with experiments related to the bridge length, ν[NHN] frequency as well as to isotope effects. Moreover they allow to understand the behaviour of such bridges owing to the possibility of analysis of the potential energy curve and distribution of protonic vibrational levels. The calculated potential energy curve for protonated 2,7-dimethoxy-DMAN is shown in Fig. 14. The MP2 barrier height is 462 cm^{-1} corresponding to 1.32 $kcal \cdot mol^{-1}$ that means that zero point energy level for $[NHN]^+$ is above the barrier. All data related to protonated 2,7-dimethoxy-DMAN are collected in Table 2. From the data in Table 2 it clearly follows that anharmonicity expressed in Eq. 10 is highly negative with unusually high frequency isotopic ratio.

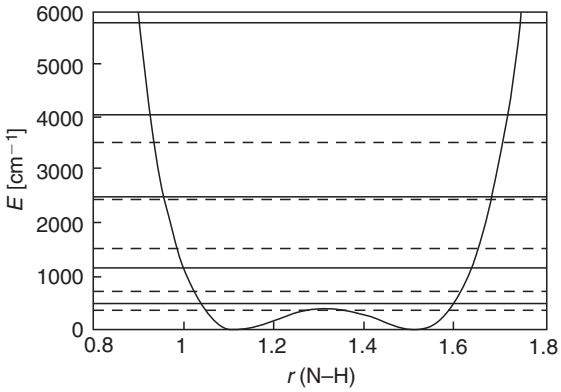

Figure 14. Calculated MP2 one-dimensional potential for protonated 2,7-dimethoxy-DMAN with indicated ν[NHN]$^+$ (solid lines) and ν[NDN]$^+$ (dashed lines) energy levels, reprinted from Ref. [52] by permission granted by the American Chemical Society.

The behaviour of protonated 2,7-dimethoxy-DMAN is similar to that of other protonated 2,7-disubstituted DMANs as shown in Table 3. The data in this table demonstrate that [NHN]$^+$ bridge is sensitive to the environment expressed in the buttressing effect exerted by various substituents in positions 2,7. This is well reflected in the geometry of molecules.

It is worth mentioning here that in the case of charge assisted [NHN]$^+$ hydrogen bonds there was reported only one system with single symmetrical potential, namely protonated 1,6-diazabicyclo[4.4.4]tetradecane [54]. In this case the N$\cdots$N distance is equal to 2.526(3) Å, the shortest known so far. The single minimum potential was confirmed based on primary H/D isotope

Table 2. Theoretically predicted anharmonic ν[NHN]$^+$ and ν[NDN]$^+$ frequencies for protonated 2,7-dimethoxy-DMAN compared to the experimental results, along with the ISR, X_{12} and barrier height values

	ν[NHN]$^+$(cm^{-1})	ν[NDN]$^+$(cm^{-1})	ISR = ν(H)/ν(D)	$-X_{12}$(cm^{-1})	Barrier height (cm^{-1})
DFT	665	331	2.01	326	475
MP2	692	352	1.97	305	462
Expt.	488	235	2.08		

Table 3. Geometrical and spectroscopic characteristics of protonated 2,7-X_2 derivatives of DMAN

	$\angle C_1C_2X$ (deg)	$\angle C_3C_2X$ (deg)	d(N$\cdots$N) Å	ν[NHN] (cm^{-1})	ISR
2,7-Br_2	124.7(2)	113.4(2)	2.547(3)	560	1.65
2,7-Cl_2	122.8(2)	115.4(2)	2.561(3)	530	1.80
2,7-$(OCH_3)_2$	116.0(2)	123.2(3)	2.567(3)	488	2.08

effect in NMR spectra. In agreement with that the $\nu[NHN]^+$ broad absorption band centred at ca. $1000\,cm^{-1}$ is observed.

It was recently evidenced [55] that also very short OHO hydrogen bonds reveal a low-barrier double-well potential. This was shown in the case of hydrogen bond with the length of 2.393 Å in 4-cyano-2,2,6,6-tetramethyl-3, 5-heptanedione of C_{2v} symmetry. An unequivocal conclusion was based on detailed INS, neutron diffraction and NMR studies. The difference between the two lowest protonic vibrational levels equals to $371\,cm^{-1}$ that convincingly speaks against the single minimum potential. One should mention that in both protonated DMAN and last example of tetramethylated heptanedione the hydrogen bonds are to a large extent isolated.

11 POSSIBILITIES OF NMR SPECTROSCOPY

NMR spectroscopy provides valuable information on the structure and dynamics of the systems with hydrogen bonds, IR and NMR data substantially supplement each other. Most direct information can be derived from spectra of magnetically active nuclei of atoms, participating in hydrogen bridge and neighbouring atoms, such as ^1H,^2H,^{13}C,^{15}N,^{19}F and ^{31}P, in some cases ^{14}N and ^{17}O. Main parameters, measured in NMR spectroscopy, are chemical shifts and scalar spin–spin couplings between adjacent or closely located nuclei. The chemical shift δ is a characteristic of magnetic shielding of a nucleus by electron shell of a molecule, it is a specific characteristic of a given atom in a molecule. Scalar spin–spin coupling constant J is a characteristic of indirect interaction energy of magnetic moments of non-equivalent nuclei through electron shell of a molecule, it determines the multiplet structure of signals.

Formation of AH···B hydrogen bond leads to low-field shift of the proton signal of AH group (decrease of electron magnetic shielding), which grows with the increase of the hydrogen bond energy. Signs and values of the shifts of the signals of A and B nuclei are specific and depend on the interacting functional groups. Scalar spin–spin couplings between nuclei of proton donor and proton acceptor give valuable information about overlapping of electron clouds of partner groups upon formation of hydrogen bond. One feature of NMR spectroscopy is of fundamental importance—it is significantly larger characteristic time τ^*, compared to the optical spectroscopy. The order of magnitude of τ^* is defined by the inverse value of the quantum transitions frequencies in a system studied by the given method. For NMR spectroscopy it is about 10^{-2}–10^{-5} s for different cases; characteristic time in optical spectroscopy is of the order of 10^{-10} (microwave) to 10^{-16} (UV) regions. On one hand, this complicates NMR study of systems with dynamic equilibrium between different molecular forms (such as hydrogen bonding, tautomeric equilibrium, internal rotation), because when $\tau^* \gg \tau$, where τ is the characteristic time of chemical process, for example, the lifetime of proton between acts of exchange, in NMR spectrum only one average signal of two or more forms participating

in exchange is registered. On the other hand, this gives a unique opportunity to measure kinetic parameters of averaging processes with $\tau \approx \tau^*$, where it is possible to measure directly the lifetime of exchanging forms by NMR lineshape analysis. This can be achieved by changing the conditions of the experiment, which can influence the lifetimes, mainly temperature and concentration, but sometimes also the magnetic field strength (by using several NMR spectrometers). In this sense processes can be described as fast or slow in NMR timescale.

The experience shows that for many systems with hydrogen bond slow exchange conditions $\tau \gg \tau^{\circ}/$ down to $\tau \approx \tau^{\circ}$ are fulfilled at temperatures below 200–150 K and it is possible to detect separated signals of non-equivalent movable protons [56, 57], ^{15}N nuclei [57, 58], ^{19}F nuclei [59, 60], ^{13}C nuclei [61] and ^{31}P nuclei [62, 63]. In slow exchange regime the tremendous potential of NMR for hydrogen bond investigation is disclosed. For example, proton chemical shift range is about 20 ppm and linewidth for exchangeable protons can be as low as 5 Hz, so that the total number of independent points in ^{1}H NMR spectrum, which characterizes selectivity of the method, is around 2000 on average spectrometer. Unfortunately, possibility to measure spectra of liquid state samples at low temperatures is limited by the small number of suitable solvents. Well utilized is the freon mixture $CDF_3/CDClF_2$, which has rather high dissolving ability even for ionic compounds and low viscosity down to freezing temperature, below 100 K. 1:1 mixture freezes around 95 K and at this temperature its dielectric constant rises up to 45 [59].

12 POTENTIAL SURFACES OF COMPLEXES WITH INTERMOLECULAR HYDROGEN BOND

12.1 Complexes of Neutral Molecules

Intermolecular hydrogen bond AH$\cdots$B in solution in majority of cases is either linear or close to linear, i.e. angle θ AHB is close to 180°. The dependence of the hydrogen bond energy on the angle is weak, thus it is convenient to build two-dimensional potential energy surface in coordinates r_1(AH), r_2(HB) (or $R = r_1 + r_2$), assuming $\theta = 180^{\circ}$. If the difference $\Delta pK_a = pK_a(AH) - pK_a(HB^+)$ is close to zero, the proton transfer state $A^- \cdots HB^+$ is sufficiently populated, which allows to detect it by spectroscopic methods [64, 65]. In other words, on the potential surface of such system there are two minima, corresponding to two stationary states of the complex, which are in the dynamic equilibrium. Enthalpy difference between these two states (relative depth of potential minima) is defined experimentally using van't Hoff's equation for the temperature dependence of the monomolecular equilibrium constant, which is equal to the ratio of concentrations of two forms of complex. Measurements of the equilibrium constant can be performed using optical spectra in UV and IR regions, where characteristic time of method is much shorter than lifetime of

the complex. In NMR spectra, however, it is rarely possible to detect simultaneously resolved signals of tautomeric molecular and ionic complexes. However, for complexes of strong acids but weak proton donors in hydrogen bond the interconversion frequency of two forms in the temperature range 250–90 K can be comparable with the difference of resonance frequencies of these forms. In such systems minima of molecular and ionic complexes on the two-dimensional potential energy surface are located far away from each other and, as a consequence, are separated by the high potential barrier, which makes the lifetime of the proton in each state comparable with the characteristic NMR time. This is the case of many CH–, SH– and NH–proton donors [56]. Strong OH and many NH acids are also strong proton donors, potential barrier between two minima is lower and rate of exchange is so high that even at $\sim$100 K in NMR spectrum only average signal of molecular and ionic forms is seen. Although in these cases spectrum is less informative, equilibrium constant can be estimated from the location of the signal between two limiting positions, corresponding to molecular and ionic forms. Signals of these forms usually cannot be measured independently and their chemical shifts are obtained indirectly.

As an example, in Fig. 15 ^{1}H NMR spectra of thiophenol C_6H_5SH dissolved in freon $CHClF_2$ in the presence of triethylamine excess obtained at different temperatures are shown [56]. Upon cooling the signal 2.6 ppm of the amine's α-methylene protons shifts to low field and splits into two signals around 150 K. While temperature decreases the chemical shift of the lower field signal, assigned to the tautomeric complex, increases due to the gradual shift of the equilibrium $SH\cdots N \Leftrightarrow S^- \cdots HN^+$ to the right side. When the proton exchange between these two tautomeric forms becomes slow in the NMR timescale the signal of the bonding proton splits in to two signals, which correspond to the molecular and ionic complexes. The lineshapes and relative intensities of

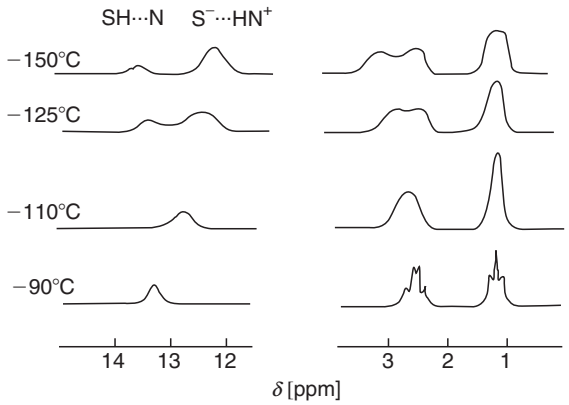

Figure 15. ^{1}H NMR spectra of thiophenol ($0.05\,mol\cdot dm^{-3}$)—triethylamine ($0.1\,mol\cdot dm^{-3}$) system in a freon $CHClF_2$ at various temperatures, reprinted from Ref. [56] by permission granted by Elsevier.

the signals do not depend on concentration. The former are modulated by the exchange rate and the latter are defined by the tautomeric equilibrium. The lineshape analysis allows to determine the lifetime of the complexes and to describe the kinetics of the proton transfer. Analogous experiments were fulfilled in a number of systems of the $RAH \cdots N(C_2H_5)_3$ type. The employed proton donors RAH, where AH = OH, NH, SH, CH, were selected in such a way that their proton-donating ability was strongly varied while the acidity stays rather unchanged. The enthalpy of the $RAH \cdots O = S(CD_3)_2$ complex estimated from IR spectra was employed as a measure of the proton-donating ability. The experimental data obtained for these systems are collected in Table 4.

The enthalpy values of the $AH \cdots N \Leftrightarrow A^- \cdots HN^+$ process are similar for the studied complexes and are between 13 and 15 $kcal \cdot mol^{-1}$. While the proton-donating ability of an acid decreases the rate of the reversible proton transfer diminishes and the activation energy increases. Thus a decrease of the potential well depth for the molecular complex causes an increase of the barrier for the proton transfer. One may conclude that the acidity of RAH defines mostly the depth of the potential well in the ionic complex while the barrier height depends on the hydrogen bond strength in the molecular complex, i.e. the distance between the bridge A, B atoms.

The equilibrium between the molecular and ionic form of hydrogen bonded complexes involving stronger proton donors such as carboxylic acids or phenols was studied using optical spectroscopy methods [64, 65]. In these structures the enthalpy of the proton transfer was found to be always negative. Since the proton transfer in solution is an exothermic process, the second well is always deeper than the first one. The proton transfer is followed by a strong reduction of the entropy due to the ordering of the solvent molecules in the solvation shell of the ionic complex having a higher dipole moment (7–10 D). The structure of strongly hydrogen-bonded complexes dramatically depends on interactions with the environment. Impressive examples are the complexes $HalH \cdot NH_3$ (Hal = Cl, Br, I) in inert gas matrices, whose structure changes qualitatively from molecular to ionic one in the row Ne, Ar, Kr, N_2 [66–68].

Table 4. The enthalpy values of hydrogen bonded complexes of acids RAH with $(CD_3)_2SO$, coalescence temperature T_c and activation energy $E^{\neq}$ of proton transfer in the complex $RAH \cdots N(C_2H_5)_3$

Acid RAH	pK_a	ΔH_{DMSO} ($kcal \cdot mol^{-1}$)	T_c (K)	$E^{\neq}$ ($kcal \cdot mol^{-1}$)
$(CH_3)_3CCOOH$	5.1	9.6	<95	<2
CH_3NHNO_2	5.1	7.0	130	2.2
C_6H_5SH	6.2	5.2	160	3.4
$(CF_3)_2CHNO_2$	5.3	4.4	220	4.7
$CH_3CH(NO_2)_2$	5.1	2.2	315	7.9
$(CF_3)_2CHCOOCH_3$	6.2	~1	>340	>10

The solvent plays an important role in the position of the tautomeric equilibrium. Indeed, such equilibrium was not ever observed in gas phase while the proton transfer in complexes formed by neutral molecules is well known, for example, in $BrH \cdot N(CH_3)_3$ as shown by NMR [69]. One may expect that perspective candidates for such study are strong CH– or SH–acids.

For systems with strong hydrogen bond NMR spectroscopy provides an important experimental criterion, which allows to distinguish the complexes with symmetric or nearly symmetric low-barrier potential from complexes with non-symmetric single-well or double-well potential with a high barrier. It is a primary $^1H/^2H$ isotope effect—the difference of signals in ^2H and ^1H NMR spectra of complexes containing deuteron and proton in hydrogen bridge $\Delta\delta \equiv \delta(A^2\underline{H}B) - \delta(A^1\underline{H}B)$. In some cases the ^3H NMR spectra of compounds enriched with tritium were obtained [70–72]. The basis of this criterion is the change of complex geometry after isotope substitution—the shortening of the bond A–D and further A–T on account of vibration anharmonicity and lesser zero point energy for heavier isotope. Then its shielding increases, hydrogen bond weakens, the distance H···B increases more than shortening of the valence bond and the length of hydrogen bridge R(A···B) increases [73, 74]. The deuteron signal is shifted to higher field in comparison with proton, the difference of their chemical shifts is negative, $\Delta\delta < 0$. The effect is small for weak hydrogen bonds, it grows with the strength of them, reaches the maximum, for OH···O bonds of about -1 ppm, then it decreases, goes through zero and becomes positive, up to $+0.3$ ppm for strongest shortest bonds; the detailed theoretical analyses are given in articles [75, 76].

It is pertinent to add that in the gas phase hydrogen bond may become shorter upon isotope substitution, $R_D(AB) < R_H(AB)$, according to the data of rotational spectroscopy [77]. This effect is maximum for weak complexes and decreases with the hydrogen bond strength, for complex $ClH \cdot NH_3$ it becomes positive. The authors [77] explained it by the opposite influence of H/D substitution on the movements with large amplitudes—stretching vibration ν_s(AH) and wagging intermolecular vibration ν_b. For weak bonds the decrease of zero point vibrations amplitude of ν_b dominates, the role of ν_s increases with the hydrogen bond strength. Since in liquid phase the positive isotope effect on chemical shifts for uncharged complexes is observed only in few cases of very strong hydrogen bond with "shared" proton, it is believed that in conditions of polar solvent the influence of zero point vibrations on ν_b mode on hydrogen bond geometry is insignificant.

In symmetric single minimum potential proton as well as deuteron and triton is located in the centre of bridge, but because of lesser energy of zero-point vibrations and lesser distance between heavy nuclei the amplitude of zero-point vibrations for ^2H and ^3H is less than for ^1H, and average over wave functions of ground state values of their chemical shift proves to be larger, the isotope effect $\Delta\delta > 0$ [70, 94]. When the minimum moves from the centre of bridge the potential curve becomes asymmetric, the distance r_1(AD) becomes less than

r_1(AH) and the opposite influence of anharmonicity on the hydrogen bond strength in H- and D-forms appears, the total effect diminishes. The $\Delta\delta$ value goes through zero, becomes positive and increases [78, 79].

Exclusively strong hydrogen bond, probably the strongest detected up to date between two neutral molecules, is formed in a polar solution between FH and 2,4,6-trimethylpyridine (collidine) [57]. In a $CDF_3/CDClF_2$ freon mixture geometry of this bond dramatically depends on temperature. At 190 K the bond is of the molecular type and H is located closer to F than to N. The single well potential curve is asymmetric and the primary isotope effect is negative. Upon cooling $\Delta\delta$ becomes positive, goes through the maximum of 0.27 ppm at 145 K and then decreases again down to 0.2–0.1 ppm at 100 K. That means that the F–H···N bridge contracts first and then lengthens again. The driving force for this contraction is an increase of the solvent polarity due to cooling [59]. The local electric field increases upon cooling because of the ordering of the solvent molecules solvated the complex. This field induces in the complex an extra dipole moment due to the proton transfer from F to N. Thus, the F···H distance increases gradually while the H···N one contracts. We will call the proton position at which the N···F distance is the smallest one as the "quasi-midpoint." For asymmetric AH···B complexes this point does not necessarily coincide with the geometrical centre of the hydrogen bridge [58]. Further increasing of the dipole moment demands an increase of the N···F distance. Thus, upon cooling geometry of the FH···collidine complex changes gradually from the molecular structure FH···N to the ionic one $F^- \cdots HN^+$ [80].

By using empirical correlation between spectroscopic and geometric characteristics of complex it was shown that the primary isotope effect changes sign when the minimum of the potential curve shifts from the quasi-midpoint by more than $\sim$0.06 Å in both sides [57].

Information about the electronic structure of strong hydrogen bond may be obtained from the structure of the NMR signal of the bonding proton. In the $^{19}F \cdot ^{1}H \cdot ^{15}N$ bridge all nuclei have the spin 1/2. Their mutual interaction through the three-centre four-electrons bond is shown in Fig. 16 [57]. The proton signal is a doublet of doublets whose splitting constants depend on the proton position in the bridge. At high temperatures the proton is strongly coupled to the fluorine, $^1J_{FH} = 88$ Hz at 180 K. Due to the proton transfer upon cooling this coupling reduces down to 45 Hz near the quasi-midpoint and finally becomes immeasurably small, less than 10 Hz. In contrast, the proton–nitrogen coupling increases upon cooling. It is about -43 Hz at 170 K, becomes equal to $^1J_{FH}$ near the quasi-midpoint and about -55 Hz at 112 K. The coupling constant between the nitrogen and the fluorine nuclei over the hydrogen bridge does not change much in the inspected temperature interval and is about -96 Hz.

The results of theoretical analysis of a similar complex perfectly correlate with the experimental data and explain the observed effects in detail [81]. It is shown that the strong changes of the $^1J_{FH}$ and $^1J_{HN}$ coupling constants are

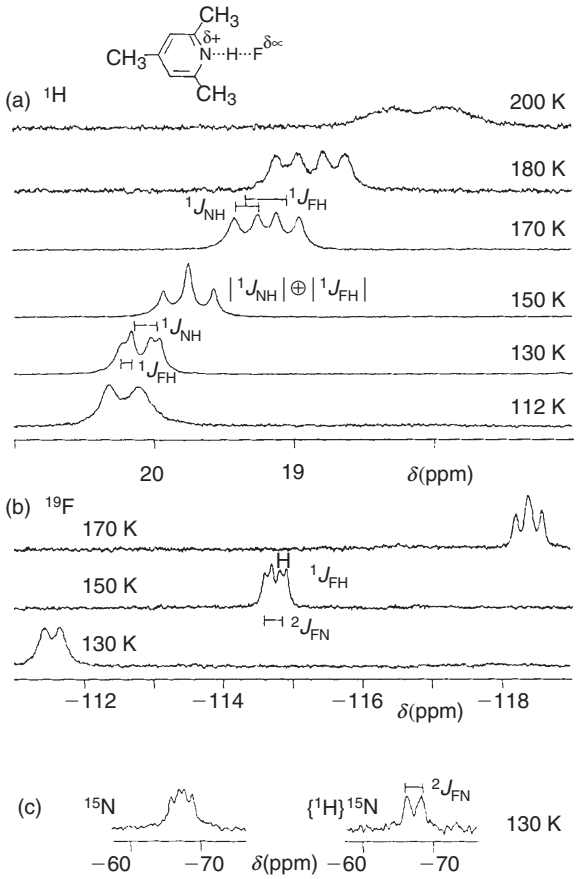

Figure 16. (*a*) ^{1}H NMR signals of the hydrogen bond proton of the 1:1 complex between collidine-^{15}N and HF in $CDF_3/CDClF_2$ of a sample containing a 10-fold excess of collidine; (*b*) ^{19}F NMR spectra of the same sample (c) ^{15}N spectra with and without proton decoupling at 130 K of a sample containing a 7-fold excess of collidine, reprinted from Ref. [57] by permission granted by the American Chemical Society.

caused by a monotonous increase of the F···H distance and the corresponding decrease of the H···N distance near the quasi-midpoint or the proton-shared bond where the F···N distance does not change much. In all cases the Fermi contact contribution is mostly responsible for the coupling with the exception of the shortest F···H distances when the paramagnetic spin–orbit contribution plays a certain role.

A monotonous increase of the potential curve asymmetry is observed for complexes of carboxylic acids with collidine having in the freon mixture the ionic structure at 120–130 K. Here $^{1}J_{HN}$ is about −65 Hz for acetic acid, 87 Hz for 2-nitrobenzoic acid and up to −90 and −92 Hz for HCl and HBF_4 [82]. The

structure of these complexes strongly depends on the local electric field and may be dramatically changed in crystal where the dielectric constant $\varepsilon \approx 5$ in contrast to ca. 30 in freon. While the crystalline collidine–HCl complex has the ionic structure as well, the benzoic acid forms with collidine in the solid state molecular complex. As a result the difference in the nitrogen chemical shifts in ^{15}N NMR spectra of the latter complex obtained in the freon mixture and crystal is about 60 ppm.

The important regularities were obtained in the study of spectra of complexes with hydrogen bond AH $\cdots$ ^{15}N on nuclei ^{15}N of isotopically enriched aromatic bases pyridine and collidine. When proton-donating ability of an acid AH increases the ^{15}N chemical shift monotonously moves towards high field approaching to limiting value, characteristic for a free cation H–^{15}N^{+}, in contrast to the chemical shift of proton which passes through the maximum near quasi-midpoint. Thus the ^{15}N chemical shift may be used to detect the minimum on the proton's potential surface. In this row of complexes the secondary isotope effect $\Delta\delta(\mathrm{N}) \equiv \delta(\mathrm{AD\underline{N}}) - \delta(\mathrm{AH\underline{N}})$ has the shape of dispersion curve, i.e. it has the maximum in region of strong molecular complexes, goes through zero near quasi-midpoint and then has minimum in region of strong hydrogen bonded zwitterionic complexes [23, 57, 78]. These features help to describe in detail the structure of a hydrogen bonded complex and the shape of its potential surface. It is pertinent to mention here the results of Rospenk et al. [83], where the secondary H/D isotope effect was measured on ^{13}C nuclei of phenyl ring in the row of Mannich bases, substituted 2-$CH_2N(C_2H_5)_2$-phenols. The non-linear intramolecular hydrogen bond OH $\cdots$ N(sp^3) exists in these compounds, the strength of which can be varied in wide limits by introducing substitutes in phenyl ring. It was found that when acidity of OH group increases the isotope effect on carbon atom C1OH, $\delta_C(\mathrm{D}) - \delta_C(\mathrm{H})$, changes analogously (with opposite sign) to the secondary isotope effect on nitrogen atom in intermolecular hydrogen bond OH $\cdots$ ^{15}N(sp^2); it goes through zero near quasi-midpoint and has maximum and minimum on both sides of this point. One can think that such behaviour may be rather typical for complexes with strong hydrogen bonds.

12.2 Complexes with Participation of Ions

Very strong bonds are formed between neutral and charged particles—charge assisted hydrogen bonds [84], complexes of neutral proton donors with anions A^- and of neutral acceptors with cations BH^+. Potential surface of these complexes may be single minimum or double minimum, in dependence on electronegativity of heavy atoms [85, 86]. The potential surface of a centrosymmetrical anion $[AHA]^-$ or cation $[BHB]^+$ has the simplest shape. The hydrodifluoride ion $[FHF]^-$ is most extensively studied experimentally and theoretically, one can assume it to be the limiting case of hydrogen bond with maximum energy 45.8 kcal $\cdot$ mol^{-1} [21, 87–89]. As evidenced by X-ray diffraction, vibrational and NMR spectroscopy, this anion in gas, crystal and solution

has centrosymmetric structure, so that its potential surface has one minimum. In deuterated anion the distance $R(F\cdots F)$ diminishes in crystal by $\sim$0.004 Å [90], in gas by $\sim$0.005 Å [91]. Therewith the primary isotope effect is positive, + 0.32 ppm, and secondary isotope effect is negative, $\delta(\underline{F}D\underline{F}) - \delta(\underline{F}H\underline{F}) = -0.37$ ppm [92, 93]. The qualitative treatment was carried out in Refs. [78, 94]; the explanation is given on a basis of comparison of the width of probability density distribution of proton and deuteron in the ground vibrational state (Fig. 17). The thorough analysis of the influence of vibrational effects on NMR spectra of isotope forms of $[FHF]^-$ anion is accomplished [21]. It is shown that for centrosymmetric ion the contribution of amplitudes of two proton vibrations, antisymmetric and bending, plays the determining role. The contribution of symmetric vibration (the change of effective length of hydrogen bond on deuteration) is negligibly small. The experimentally observed opposite signs of isotope effect on hydrogen and fluorine nuclei resulted in the dominating role of stretching vibration in the first case, and of bending proton vibration in the second case. When passing to complexes with asymmetric proton location, the anharmonic contribution of stretching proton vibration appears and increases, as a result of which the primary H/D isotope effect decreases and changes its sign.

The NMR study of the strong hydrogen bond $^{15}N \cdot H \cdot ^{15}N$ in a complex $(R{-}C{\equiv}N\cdots H\cdots N{\equiv}C{-}R)\cdot X^+$ in solid state led to the similar conclusions

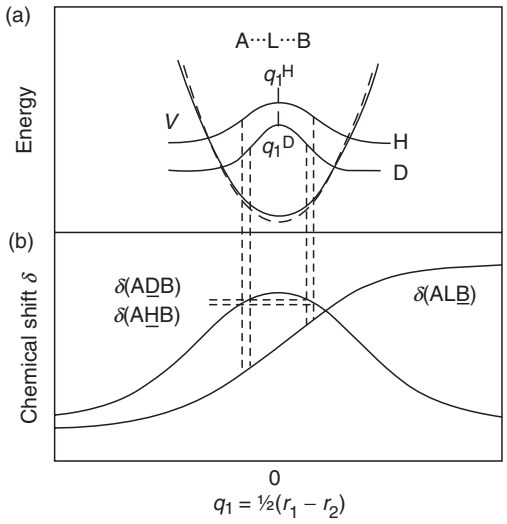

Figure 17. (*a*) One-dimensional potential curve and squared ground state wave function (schematically) of a symmetric single-well hydrogen bond ALB, L = H, D. (*b*) Chemical shifts δ(ALB) (schematically) of B and L as a function of q_1. The average chemical shift of D is larger than for H because of the maximum of δ(ALB) and the narrower wave function of D compared with H. By contrast, as δ(ALB) is a linear function of q_1, $\delta(AHB) = \delta(ADB)$, reprinted from Ref. [78] by permission granted by Wiley-VCh.

[23, 79, 80]. Two compounds were studied with symmetric and asymmetric position of a proton between nitrogen atoms ($X^+ = AsPh_4^+$ and NPr_4^+). On H/D substitution the distance $R(N\cdots N)$ in the first complex diminishes from 2.62 to 2.60 Å, and in the second one it increases from 2.68 to 2.71 Å. The distances r_1 and r_2 in the first complex remain equal, but in the second complex the length of valence bond $r_1(N{-}H)$1.16Å decreases by 0.03 Å, and the length of hydrogen bond $r_2(H\cdots N)$1.49 Å increases by 0.06 Å. Chemical shift of nitrogens signal in the spectrum of symmetrical complex is hardly changed on deuteration, but in the spectrum of asymmetric complex two nitrogen signals shift in opposite directions, the distance between them increases. The secondary isotope effect on nitrogen qualitatively reproduces the primary geometric isotope effect on proton transfer coordinate $q_1 = 1/2(r_1 - r_2)$. Theoretical consideration of a model linear system $(C{\equiv}N\cdots H\cdots N{\equiv}C)^- \cdot Li^+$, in which the interaction with a cation models the perturbation by external electric field, showed that on approaching a cation the symmetric low-barrier potential loses its symmetry, becomes non-symmetric and its minimum gradually shifts towards one of nitrogen atoms. Hence, the negative H/D effect on geometry (shortening of R(AB) length on deuteration) and positive effect on hydrogen chemical shift (low-field shift of deuteron signal in comparison with proton) allow to identify the systems with single-well potential, with central or nearly central proton location. The NMR criterion is more valuable than the structural one, since it is applicable not only to crystals but to neat liquids and solutions as well.

An interesting approach providing a possibility of measurements of geometric parameters of complexes with hydrogen bond in solutions by the method of nuclear magnetic relaxation is proposed by authors [95, 96]. The measurements of longitudinal magnetic relaxation time T_1 of heavy nuclei were carried out in freon solutions at temperatures 100–150 K in conditions of slow proton and molecular exchange for complexes $FH\cdots{}^{15}NCH$ and $[FHF]^-$ in three (H,D,T) isotopic modifications. Using these data the ratios of distances $r_1(AT)/r_1(AH)$ and $r_2(TB)/r_2(HB)$ in these complexes were calculated. It was found that in complex $FH\cdots N$ the replacement of hydrogen by tritium results in shortening of F–H bond and in lengthening of hydrogen bond $H\cdots N$, the distance $R(F\cdots N)$ increases by 0.02 Å. But in complex $[FHF]^-$ the reverse effect is observed—the diminution of the distance between heavy atoms. It evidences for some strengthening of hydrogen bond, which manifests itself in positive isotope effect on chemical shift of bridging proton. The obtained value of shortening of $R(F\cdots F)$ distance 0.008 Å is in accordance with the value of geometric isotope effect for isolated anion in gas phase, found from IR spectrum [90], so that this value is practically insensitive to the phase state and the presence of a counter-ion.

In strong hydrogen bond [N·H·N] in homoconjugated bis-collidinium cation in freon solution the proton signal 19.93 ppm is a triplet with a constant

$^1J_{NH} = 40$ Hz; the primary isotope effect is $\Delta\delta = -0.81$ ppm [93]. This demonstrates the double-well symmetric potential with fast migration of a proton between two equivalent positions (in slightly disturbed collidinium ion the proton signal of NH^+ group is a doublet with a constant $^1J_{NH} = 85$ Hz). Similar situation is in protonated proton sponges such like in 1,8-*bis*(dimethylamino)-2,7-dimethoxy naphthalene [97]. $^1H/^2H$ primary isotope effect convincingly shows a double-well potential although the NHN bridge is very short, 2.567(3) Å.

In complexes of carboxylic acids with their anions $[AHA]^-$ hydrogen bond is weaker than in anion $[FHF]^-$, and the results of experimental and theoretical studies point to double-well potential of proton in a bridge $[OHO]^-$. The primary isotope effect in ^1H NMR spectrum of hydrogen diacetate anion according to Refs. [61, 93] is negative and large, $\Delta\delta = -0.62$ ppm. An additional information about O·H·O bond is obtained from ^{13}C spectra of carbon atoms adjoining to the hydrogen bridge. The secondary isotope effect on ^{13}C nucleus of carboxylic group $\delta_C(D) = \delta_C(H) = -0.20$ ppm is negative; also, it repeats the sign of a primary effect. The authors concluded that the proton potential in this anion is symmetric and has two wells, the same result gives the theoretical analysis. The interaction with solvate shell results in fluctuations of instantaneous form of potential but does not change its double-well character. The fast proton exchange between two wells averages the signals of carboxylic carbon and only one line is revealed in the spectrum [61].

In the row of acetic acid complexes with anions $CH_3CO_2^-$, $CH_2ClCO_2^-$, $CHCl_2CO_2^-$, $CCl_3CO_2^-$ the OH···O hydrogen bond weakens rapidly as one can see from the ^1H chemical shifts—19.25, 16.91, 15.64, 12.04 ppm [98]. In the ^{13}C NMR spectra of asymmetrical complexes $[A_1 \cdot H \cdot A_2]^-$ of this row the signals of two carboxylic carbons are observed separately, the secondary isotope effect on carbon atom of acetic acid decreases rapidly in this row (−0.357, −0.234, −0.100 ppm) and exceeds significantly the secondary isotope effect on carbon of chlorosubstituted anion (−0.053, −0.034, −0.100 ppm). It shows on hydrogen bond OH···O in strongly asymmetric single-well potential [98].

13 INTRAMOLECULAR HYDROGEN BOND

13.1 Enols of β-Diketones

Intramolecular hydrogen bond, as a rule, is non-linear, and the dependence of the energy of a system on the angle AHB θ should be accounted for in building one-dimensional and two-dimensional potential surfaces. The authors [99] advanced a new approach for determination of the type of potential in intramolecular hydrogen bond O·H·O in enols of β-diketones. They suggested the method of representation in one-dimensional form of potential curves describing the profile of proton movement between two oxygen atoms. The difference $r_1(O–H) - r_2(H \cdots O)$ at different distances R and angles θ is used as a reaction

coordinate; it was calculated employing Lippincott–Schröder equation. The obtained curves are classified by form and symmetry.

The potential curves of *cis*-enolic form of β-diketones are difficult ones for classification cases of resonance-assisted hydrogen bonds, since parameters of the surface may change strongly for different substituents X, Y, Z. The surface may have either one minimum localized near one of oxygen atoms, or in the centre of the bridge, or two minima of equal (X = Y) or different depth (X ≠ Y). Double-minimum surface corresponds to the existence of two tautomers, being in movable equilibrium with one another. The high rate of mutual conversion gives rise to averaging of signals of two forms, so that it is impossible to distinguish different forms by direct experiment, and one is led to use the indirect arguments. Many examples of such works are given in the review [100]. The important criterion is the temperature dependence of chemical shifts of nuclei forming the hydrogen bridge and adjacent nuclei, mainly ^{13}C, and of scalar spin coupling constants. In case of non-symmetric compounds, X ≠ Y, one may expect existence of two forms with different energies, and if the energy difference is not very large, the change of state population in operating temperature interval can be measured by the position of averaged signal of these forms. Approximation of $\delta(T)$ dependence by van't Hoff function allows to find unknown parameters, enthalpy and entropy of tautomeric transfer and chemical shifts of each tautomer. Sometimes it is possible to use the independent values of chemical shifts of individual tautomers taken from spectra of model compounds, then the precision may be increased. In a similar way the measurements of tautomeric equilibrium may be carried out by temperature dependence of scalar spin coupling constant of movable proton and adjacent nucleus ^{17}O, ^{13}C or proton ^{1}H if X = H. Enthalpy difference measured for different dicarbonyl compounds reaches 1.0 kcal · mol^{-1}, the precision of measurement of relative concentration of tautomers is of few percent [100]. If energy difference is large the fraction of dominating tautomer is indistinguishable from unity and the potential with a good approximation can be assumed the single minimum one (Scheme 1) [99].

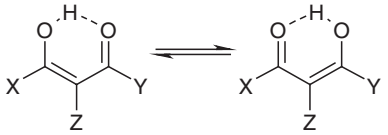

Scheme 1

For symmetric substitution, X = Y, the equilibrium is degenerate, two wells have equal depths and the population of both states is equal at any temperature. In this case chemical shift does not depend on temperature and scalar spin coupling constant has one half value of the full one. Such behaviour allows to identify the systems with close values of depth of two wells and fast in NMR scale proton migration between them. For example, in ^{1}H NMR spectrum of enol form of malonedialdehyde (X = Y = Z = H) at 170 K the signal of OH

proton is a triplet on account of average spin–spin interaction with two formyl protons. The effective constant $^3J_{OH,H}$ is equal to average value of interaction constants with these protons $1/2\ (13 + 0) = 6.5$ Hz.

It should be noted that in enols of β-diketones (acetyl- and benzoylacetone, dibenzoylmethane) the largest primary negative isotope effect is observed, for deuterium between −0.6 and −0.7 ppm and for tritium between −0.8 and −1.0 ppm [70, 71]. It corroborates the double-well character of proton potential in compounds of this group. Even in the shortest intramolecular OHO bridge in 4-cyano-2,2,6, 6-tetramethyl-3,5-heptanedione [55], of 2.393 Å length (see Sect. 10) it was evidenced, based on neutron diffraction and inelastic scattering, a double minimum potential with very low barrier. The authors of the cited paper believe the existence of single minimum potential to be unlikely in compounds of this type.

13.2 Anions of Dicarboxylic Acids

The study of isotope effects in NMR spectra of the other classical examples of the strong intramolecular hydrogen bond with single minimum potential, the hydrogen maleate anion MA and its methyl substituted, hydrogen citraconate anion CA, illustrates the high sensitivity of ^{13}C spectra to the small changes of potential curve of a proton [93, 98]. The positive primary isotope effect in both anions, +0.051 and +0.162 ppm, shows on the low-barrier hydrogen bond with a proton location in the centre of a bond for MA and, for symmetry reasons, slightly shifted from the centre for CA; the proton signal of CA is shifted to low field by 0.075 ppm in comparison with MA (20.915 and 20.840 ppm correspondingly). This shift, as well as considerable difference in primary isotope effects, is likely a consequence of the shorter distance $R(O\cdots O)$ in CA. Symmetrical MA gives in ^{13}C spectrum only one signal 171.057 ppm of carboxylic carbon, after partial deuteration the second signal of D-form appears shifted to higher field by 0.069 ppm. But in the spectrum of CA two carboxylic carbons give different signals 171.578 and 171.265 ppm (Fig. 18). The secondary isotope effect on these nuclei differs significantly, on C1 it is less than in MA, −0.013 ppm, and on C4 it is larger, −0.087 ppm. This means that in asymmetric potential well of CA proton is located slightly closer to carbon C4. It is appropriate to add that the sign of secondary isotope effect on nuclei C2 and C3 is different, −0.25 and +0.16 ppm correspondingly. The quantum-chemical consideration could help to understand the nature of these shifts.

14 SYNCHRONOUS TRANSFER OF PROTONS IN CYCLIC COMPLEXES WITH SEVERAL HYDROGEN BONDS

Certain compounds susceptible to self-association form stable cyclic structures with several hydrogen bonds—dimers, trimers, etc. Many-dimensional potential surface of such systems has two minima, corresponding to two

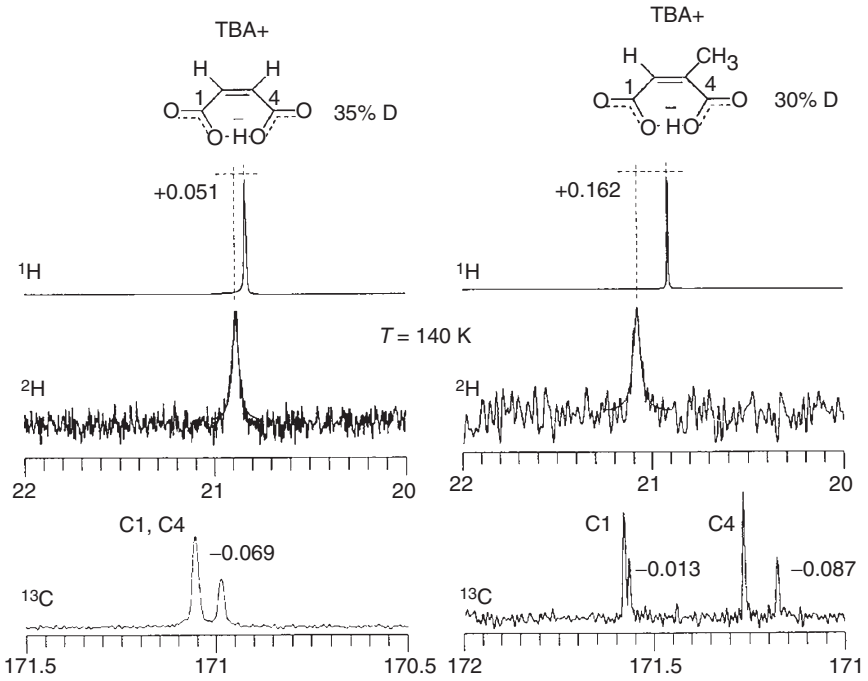

Figure 18. ^{1}H,^{2}H and ^{13}C NMR spectra of partially deuterated hydrogen maleate and hydrogen citraconate in $CDF_3/CDClF_2$ (tetrabutylammonium salts), according to Ref. [98].

mirror-symmetrical forms of a complex. These forms are in degenerate equilibrium with one another, the exchange between them occurs through synchronous transfer of protons along hydrogen bonds. The most stable structures are stabilized by resonance interaction in π-electron system in a cycle closed by hydrogen bond (resonance-assisted hydrogen bond [84], therefore the coordinates of heavy atoms also change substantially during the proton transfer. The example of such systems may be well studied by methods of NMR cyclic dimers of carboxylic acids [101–103], and cyclic dimers, trimers and tetramers of pyrazoles [104, 105]. The measurements of the process kinetics enabled to estimate the activation energy of tautomeric transfer—the barrier height of the reaction path profile. At low temperatures the influence of tunnelling reveals itself, the value of kinetic isotope effect for H/D/T forms is determined. Theoretical analysis of the potential surface shape of carboxylic acid dimers showed that the low frequency vibrations make a noticeable contribution to the reaction coordinate of synchronous transfer of protons, an adequate description of experimental results can be realized by the use of at least four-dimensional potential surface [102]. The authors [104] found that the shortening of distances between heavy atoms in hydrogen bridges, the

"shrinking" of a ring, occurs at synchronous transfer of protons in cyclic complexes of pyrazoles; it also evidences the valuable participation of the heavy atom movement in the reaction coordinate.

ACKNOWLEDGMENTS

This research has been supported by the Russian Foundation of Basic Research, grants 03-03-04009 and 05-03-33235. A financial support by the Polish Ministry of Science and Informatics (Grant 4TO9A 05125) is also acknowledged.

REFERENCES

1. G. Fogarasi and P. Pulay (1985) in *Ab Initio Calculation of Force Fields and Vibrational Spectra*, J. Durig (ed.), Vibrational Spectra and Structure, Vol. **14**, Elsevier Science, Amsterdam, p. 125.
2. A. P. Scott and L. Radom (1996) *J. Phys. Chem*. **100**, 16502.
3. O. Henri-Rousseau, P. Blaise and D. Chamma (2002) *Adv. Chem. Phys*. **121**, 241.
4. C. L. Perrin and J. B. Nielson (1997) *Annu. Rev. Phys. Chem*. **48**, 511.
5. Z. Mielke and L. Sobczyk (2005) in *Vibrational Isotope Effects in Hydrogen Bonds*, A. Kohen and H.-H. Limbach (eds.), Isotope Effects in Biology and Chemistry, Taylor & Francis, Boca Raton, 2006, pp. 281–304.
6. A. Warshel (1991) *Computer Modeling of Chemical Reactions in Enzymes and Solution* (J. Wiley, New York).
7. E. R. Lippincott and R. Schröder (1955) *J. Chem. Phys*. **23**, 1099.
8. E. Matsushita and T. Matsubara (1982) *Progr. Theor. Phys*. **67**, 1.
9. T. Saitoh, K. Mori and R. Itoh (1981) *Chem. Phys*. **60**, 161.
10. M. Rospenk and Th. Zeegers-Huyskens (1997) *J. Phys. Chem. A* **101**, 8428.
11. R. L. Somorjai and D. F. Hornig (1962) *J. Chem. Phys*. **36**, 1980.
12. H. Romanowski and L. Sobczyk (1977) *Chem. Phys*. **19**, 361.
13. L. Sobczyk (1996) *Mol. Phys. Rep*. **14**, 19.
14. Y. Guissani and H. Ratajczak (1981) *Chem. Phys*. **62**, 319.
15. J. Laane (1971) *J. Chem. Phys*. **55**, 2514.
16. M. Barroso, L. G. Arnaut and S. J. Formosinho (2005) *Chem. Phys. Chem*. **6**, 363.
17. J. Florián (2002) *J. Phys. Chem. A* **106**, 5046.
18. J. Stare and J. Mavri (2002) *Comput. Phys. Comm*. **143**, 222.
19. C. C. Marston and G. G. Balint-Kurti (1989) *J. Chem. Phys*. **91**, 3571.
20. N. S. Golubev, I. G. Shenderovich, P. M. Tolstoy and D. N. Shchepkin (2004) *J. Mol. Struct*. **697**, 9.
21. N. S. Golubev, S. M. Melikova, D. N. Shchepkin, I. G. Shenderovich, P. M. Tolstoy and G. S. Denisov (2003) *Z. Phys. Chem*. **217**, 1549.
22. I. G. Shenderovich, S. N. Smirnov, G. S. Denisov, V. A. Gindin, N. S. Golubev, A. Dunger, R. Reibke, S. Kirpekar, O. L. Malkina and H.-H. Limbach (1998) *Ber. Bunsenges. Phys. Chem*. **102**, 422.
23. H. Benedict, H.-H. Limbach, M. Wehlan, W. P. Fehlhammer, N. S. Golubev and R. Janoschek (1998) *J. Am. Chem. Soc*. **120**, 2939.
24. T. Dziembowska and Z. Rozwadowski (2001) *Curr. Org. Chem*. **5**, 289.
25. P. E. Hansen (1996) *Isotope Effects on Chemical Shift as a Tool in Structural Studies* (Roskilde Univ. Press, Roskilde).
26. J. Stare, A. Jezierska, G. Ambrožič, I. J. Košir, J. Kidrič, A. Koll, J. Mavri and D. Hadži (2004) *J. Am. Chem. Soc*. **126**, 4437.

27. J. Tomasi and M. Persico (1994) *Chem. Rev*. **94**, 2027.
28. R. M. Czerwinski, T. K. Harris, M. A. Massiah, A. S. Mildvan and C. P. Whitman (2001) *Biochemistry* **40**, 1984.
29. J. Stare, J. Panek, D. Hadži and J. Mavri *J. Phys. Chem. A*, to be submitted.
30. R. Car and M. Parrinello (1985) *Phys. Rev. Lett*. **55**, 2471.
31. D. Sebastiani and U. Rothlisberger (2004) in *Advances in Density-functional-based Modeling Techniques—Recent Extensions of the Car-Parrinello Approach*, P. Carloni and F. Alber (eds.), Quantum Medicinal Chemistry, J. Wiley, New York.
32. J. Stare, J. Panek, J. Eckert, J. Mavri and D. Hadži, to be published.
33. H. J. C. Berendsen and J. Mavri (1993) *J. Phys. Chem*. **97**, 13464.
34. J. Mavri and J. Grdadolnik (2001) *J. Phys. Chem. A* **105**, 2045.
35. N. Došlić, O. Kühn, J. Manz and K. Sundermann (1998) *J. Phys. Chem. A* **102**, 9645.
36. S. B. Braun-Sand, M. Olsson, J. Mavri and A. Warshel, in *Computer Simulation of Proton Transfer in Enzymes and Solution*, R. Schowen, J. P. Klinman and J. T. Hynes (eds.), Handbook of Hydrogen Transfer, in press.
37. C. Sandorfy (1976) in *Anharmonicity and Hydrogen Bonding*, P. Schuster, G. Zundel and C. Sandorfy (eds.), The Hydrogen Bond. Recent Developments in Theory and Experiments, Vol. **2**, North-Holland, Amsterdam, p. 613.
38. C. Sándorfy (1995) *Bull. Pol. Acad. Sci. Chem*. **43**, 7.
39. A. Witkowski (1967) *J. Chem. Phys*. **47**, 3645.
40. Y. Marechal and A. Witkowski (1968) *J. Chem. Phys*. **48**, 3697.
41. M. J. Wójcik (1976) *Int. J. Quant. Chem*. **10**, 747.
42. M. Boczar, K. Szczeponek, M. J. Wójcik and C. Paluszkiewicz (2004) *J. Mol. Struct*. **700**, 39.
43. R. E. Asfin, G. S. Denisov, D. M. Poplevchenkov, K. G. Tokhadze and T. V. Velikanova (2002) *Pol. J. Chem*. **76**, 1223.
44. D. Hadži and S. Bratos (1976) in *Vibrational Spectroscopy of the Hydrogen Bond*, P. Schuster, G. Zundel and C. Sandorfy (eds.), The Hydrogen Bond. Recent Developments in Theory and Experiments, Vol. **2**, North-Holland, Amsterdam, p. 565.
45. G. Zundel (2000) *Adv. Chem. Phys*. **111**, 1.
46. N. D. Sokolov, M. V. Vener and V. A. Savel'ev (1990) *J. Mol. Struct*. **222**, 365.
47. S. Bratos (1975) *J. Chem. Phys*. **63**, 3499.
48. M. Rospenk and L. Sobczyk (2006) *Asian Chem. Lett*. 10(1–2), 7.
49. J. Rossarie, J.-P. Gallas, C. Binet and R. Romanet (1977) *J. Chim. Phys*. **74**, 188.
50. Th. Zeegers-Huyskens and L. Sobczyk (1990) *Spectrochim. Acta A* **46**, 1693.
51. A. J. Bieñko, Z. Latajka, W. Sawka-Dobrowolska, L. Sobczyk, V. A. Ozeryanskii, A. F. Pozharskii, E. Grech and J. Nowicka-Scheibe (2003) *J. Chem. Phys*. **119**, 4313.
52. V. A. Ozeryanskii, A. F. Pozharskii, A. J. Bieñko, W. Sawka-Dobrowolska and L. Sobczyk (2005) *J. Phys. Chem. A* **109**, 1637.
53. L. Sobczyk (2005) *Khim. Fiz*. **24**, 1.
54. R. W. Alder, R. E. Moss and R. B. Sessions (1983) *J. Chem. Soc. Chem. Commun*. 1000.
55. J. A. Belot, J. Clark, J. A. Cowan, G. S. Harbison, A. I. Kolesnikov, Y.-S. Kye, A. J. Schultz, C. Silvernail and X. Zhao (2004) *J. Phys. Chem. B* **108**, 6922.
56. G. S. Denisov and N. S. Golubev (1981) *J. Mol. Struct*. **75**, 311.
57. I. G. Shenderovich, P. M. Tolstoy, N. S. Golubev, S. N. Smirnov, G. S. Denisov and H.-H. Limbach (2003) *J. Am. Chem. Soc*. **125**, 11710.
58. S. N. Smirnov, N. S. Golubev, G. S. Denisov, H. Benedict, P. Schah-Mohammedi and H.-H. Limbach (1996) *J. Am. Chem. Soc*. **118**, 4094.
59. I. G. Shenderovich, A. P. Burtsev, G. S. Denisov, N. S. Golubev and H.-H. Limbach (2001) *Magn. Reson. Chem*. **39**, S91.
60. I. G. Shenderovich, H.-H. Limbach, S. N. Smirnov, P. M. Tolstoy, G. S. Denisov and N. S. Golubev (2002) *Phys. Chem. Chem. Phys*. **4**, 5488.

61. P. M. Tolstoy, P. Schah-Mohammedi, S. N. Smirnov, N. S. Golubev, G. S. Denisov and H.-H. Limbach (2004) *J. Am. Chem. Soc*. **126**, 5621.
62. C. Detering, P. M. Tolstoy, N. S. Golubev, G. S. Denisov and H.-H. Limbach (2001) *Dokl. Phys. Chem*. **379**, 191.
63. N. S. Golubev, S. N. Smirnov and P. M. Tolstoy (2006) *Zhur. Obshch. Khim*., in press
64. M. M. Habeeb (1997) *Appl. Spectr. Rev*. **32**, 103.
65. A. Jarczewski and C. D. Hubbard (2003) *J. Mol. Struct*. **649**, 287.
66. L. Andrews, X. Wang and Z. Mielke (2001) *J. Phys. Chem. A* **105**, 6054.
67. L. Andrews and X. Wang (2001) *J. Phys. Chem. A* **105**, 6420.
68. L. Andrews and X. Wang (2001) *J. Phys. Chem. A* **105**, 7541.
69. N. S. Golubev and G. S. Denisov (1982) *Khim. Fiz*. **1**, 965.
70. L. J. Altman, D. Laungani, G. Gunnarsson, H. Wennerström and S. Forsén (1978) *J. Am. Chem. Soc*. **100**, 8264.
71. S. Bolvig, P. E. Hansen, H. Morimoto, D. Wemmer and P. Williams (2000) *Magn. Reson. Chem*. **38**, 525.
72. W. Schilf, J. P. Bloxsidge, J. R. Jones and S. Y. Lu (2004) *Magn. Reson. Chem*. **42**, 556.
73. M. Ichikawa (2000) *J. Mol. Struct*. **552**, 63.
74. H. D. Lutz and B. Engelen (2002) *Trends Appl. Spectr*. **4**, 355.
75. N. D. Sokolov, M. V. Vener and V. A. Savel'ev (1988) *J. Mol. Struct*. **177**, 93.
76. M. V. Vener (1992) *Chem. Phys*. **166**, 311.
77. A. C. Legon and D. J. Millen (1988) *Chem. Phys. Lett*. **147**, 484.
78. H.-H. Limbach, M. Pietrzak, S. Sharif, P. M. Tolstoy, I. G. Shenderovich, S. N. Smirnov, N. S. Golubev and G. S. Denisov (2004) *Chem. Eur. J.* **10**, 5195.
79. H.-H. Limbach, M. Pietrzak, H. Benedict, P. M. Tolstoy, N. S. Golubev and G. S. Denisov (2004) *J. Mol. Struct*. **706**, 115.
80. H.-H. Limbach, G. S. Denisov and N. S. Golubev (2005) in *Isotope Effects in the Biological and Chemical Sciences*, A. Kohen and H.-H. Limbach (eds.), Isotope Effects in Biology and Chemistry, CRC Press, Boca Raton, FL, USA, in press.
81. J. E. Del Bene, R. J. Bartlett and J. Elguero (2002) *Magn. Reson. Chem*. **40**, 767.
82. P. M. Tolstoy, S. N. Smirnov, I. G. Shenderovich, N. S. Golubev, G. S. Denisov and H.-H. Limbach (2004) *J. Mol. Struct*. **700**, 19.
83. M. Rospenk, A. Koll and L. Sobczyk (1995) *J. Mol. Liqu*. **67**, 63.
84. G. Gilli and P. Gilli (2000) *J. Mol. Struct*. **552**, 1.
85. S. Gronert (1993) *J. Am. Chem. Soc*. **115**, 10258.
86. S. Gronert and C. Kimura (2003) *J. Phys. Chem. A* **107**, 8932.
87. S. I. Kawahara, T. Uchiwaru and K. Taira (2001) *Chem. Phys*. **273**, 207.
88. A. M. Panich (1995) *Chem. Phys*. **196**, 511.
89. E. A. Moore, A. Healy, M. Mortimer and N. F. Peirson (1993) *J. Mol. Struct. (Theochem)* **285**, 229.
90. W. C. Hamilton and J. A. Ibers (1968) *Hydrogen Bonding in Solids* (W. A. Benjamin, Inc, New York-Amsterdam).
91. K. Kawaguchi and E. Hirota (1986) *J. Chem. Phys*. **84**, 2953.
92. F. Y. Fujiwara and J. S. Martin (1974) *J. Am. Chem. Soc*. **96**, 7625.
93. P. Schah-Mohammedi, I. G. Shenderovich, C. Detering, H.-H. Limbach, P. M. Tolstoy, S. N. Smirnov, G. S. Denisov and N. S. Golubev (2000) *J. Am. Chem. Soc*. **122**, 12878.
94. G. Gunnarsson, H. Wennerstrom, W. Egan and S. Forsén (1976) *Chem. Phys. Lett*. **38**, 96.
95. N. S. Golubev, D. N. Shchepkin and S. M. Melikova (2003) *Khim. Fiz*. **22**, 3.
96. G. S. Denisov, V. A. Gindin, N. S. Golubev, S. S. Ligay, D. N. Shchepkin and S. N. Smirnov (1995) *J. Mol. Liqu*. **67**, 217.
97. C. L. Perrin and B. K. Ohta (2001) *J. Am. Chem. Soc*. **123**, 6520.
98. P. M. Tolstoy (2004) *Location of the Proton in Strong Hydrogen Bonds Using Isotope Effects in* ^{13}*C NMR Spectra in Solution*, Thesis, St. Petersburg University; P. M. Tolstoy, N. S. Golubev,

G. S. Denisov and H.-H. Limbach (2003) *Deprotonation of the Carboxylic Group Monitored by H/D Isotope Effects on ^{13}C NMR Chemical Shift Measured in Slow Exchange Regime*, XV Conference-Workshop "Horizons in Hydrogen Bond Research", Berlin, Germany, 16–20.09.2003.
99. P. Gilli, V. Bertolasi, L. Pretto, V. Ferretti and G. Gilli (2004) *J. Am. Chem. Soc*. **126**, 3845.
100. A. I. Koltsov (1998) *J. Mol. Struct*. **444**, 1.
101. B. H. Meier, F. Graf and R. R. Ernst (1982) *J. Chem. Phys*. **76**, 767.
102. T. Loerting and K. R. Liedl (1998) *J. Am. Chem. Soc*. **120**, 12595.
103. Q. Xue, A. J. Horsewill, M. R. Johnson and H. P. Trommsdorff (2004) *J. Chem. Phys*. **120**, 11107.
104. O. Klein, F. Aguilar-Parrilla, J. M. Lopez, N. Jagerovic, J. Elguero and H.-H. Limbach (2004) *J. Am. Chem. Soc*. **126**, 11718.
105. H.-H. Limbach (2002) in *NMR—A Tool for the Study of the Dynamics of Hydrogen Transfer in Liquids and Solids*, D. M. Grant and R. K. Harris (eds.), Encyclopedia of Nuclear Magnetic Resonance Advances in NMR, Suppl. Vol. **9**, John Wiley & Sons, Ltd, Chichester, p. 520.